Evaluation of Mass Transport Losses in Micro-Tubular Solid Oxide Fuel Cells Anodes

by

Kristina Phillips

A Thesis Presented in Partial Fulfillment
of the Requirements for the Degree
Master of Science

Approved March 2023 by the
Graduate Supervisory Committee:

Ryan Milcarek, Chair
Patrick Phelan
Robert Wang

ARIZONA STATE UNIVERSITY

May 2023

ABSTRACT

Solid Oxide Fuel Cells (SOFCs) generate electricity using only hydrogen and oxygen and they form H_2O as the only byproduct, giving them the potential to significantly reduce carbon emissions and the impacts of global warming. In order to meet the global power demands today, SOFCs need to significantly increase their power density and improve robustness in startup and cycling operations. This study explores the impact of decreasing the anode thickness to improve the mass transport of the fuel through the anode of a micro-tubular (mT) SOFC because few studies have reported the correlation between the two. Decreasing the thickness decreases the chance for concentration overpotential which is caused by not enough of the reactants being able to reach the reaction site while products are not able to be removed quickly enough. Experiments were performed in a split tube furnace heated to 750°C with nickel-yttria stabilized zirconia (Ni-YSZ) supported cells. Pure hydrogen was supplied to the cell at rates of 10, 20, 30, and 40 mL/min while the cathode was supplied air from the environment. The cell's performance was studied using the current-voltage method to generate polarization curves and electrochemical impedance spectroscopy to create Bode and Nyquist plots. The results from the electrochemical impedance spectroscopy show a lower impedance for the frequencies pertaining to the gas diffusion in the anode for the thinner cells. This suggests that decreasing the anode thickness increases the mass transport of the gas. Additionally, through a distribution of relaxation times (DRT) analysis, the peaks vary between the two cell thicknesses at the frequencies pertaining to gas diffusion in anode-supported cells, implicating the decreased resistance created by thinning the anode layer.

ACKNOWLEDGMENTS

I would like to thank Dr. Ryan Milcarek for serving as my thesis director and giving me his guidance throughout the year. I would also like to thank Dr. Robert Wang and Dr. Patrick Phelan for serving as my committee members. Lastly, I would like to thank Brent Skabelund for his assistance in the cell fabrication and testing. I could not have gotten as many tests done without him.

TABLE OF CONTENTS

Page

Page

CHAPTER

LIST OF TABLES

Table Page

LIST OF FIGURES

Figure Page

CHAPTER 1

INTRODUCTION

Extensive research has been conducted in the past few years to create clean sources of electricity production because current sources involve burning of fossil fuels which leads to greenhouse gas production and global warming. Global warming causes intense weather phenomena such as excessive heat waves that lead to increased energy consumption (Mccarthy et al., 2010). To find a solution, extensive research has been done on fuel cells because they produce power with little to no emissions and have high efficiencies (B. Zhao et al., 2022).

Fuel cells are comprised of an anode, electrolyte, and a cathode. The cell is fed hydrogen that oxidizes as it diffuses through the anode while simultaneously, the oxygen from the air is reduced as it diffuses through the cathode. The oxygen ions flow through the electrolyte to react with the hydrogen while electrons are unable to pass through and they instead travel to an external circuit where they generate direct current. A battery generates power from a finite amount of fuel stored within the battery and once it has been exhausted, it can no longer provide power (Breeze, 2017). With a fuel cell, the fuel is provided externally so it can produce power as long as there is a source available (Breeze, 2017; O'Hayre et al., 2016).

Polymer electrolyte membrane fuel cells (PEMFC) and SOFCs are two of the most common types of fuel cells. The cells differentiate in the materials that they use for their electrolyte and electrodes. A PEMFC uses a polymer membrane for its electrolyte allowing it to operate at a lower temperature range between 60-120°C. The benefits of this are that less power and time is required to reach the operating temperature, making them suitable

for portable applications (Malik et al., 2021). The SOFC has a ceramic electrolyte that requires an operating temperature between 600-1000°C (O'Hayre et al., 2016). The benefits of a higher operating temperature are that they are able to generate power for large scale applications as well as operate on a variety of different fuels (Malik et al., 2021). There are two different designs for SOFCs, planar and tubular. A planar cell is a rectangular flat cell where the anode, electrolyte and cathode are stacked on top of each other. In a tubular cell, the layers are stacked out radially. Tubular fuel cells come in the micro-tubular size where the entire diameter of the cell is around ~ 3mm or less (R. J. Milcarek, Garrett, Wang, et al., 2016; Sammes et al., 2005). Having this small size makes them more suited for portable devices because of improved durability which results in their ability to start up rapidly compared to planar cells (R. J. Milcarek et al., 2018, 2020). Planar fuel cells, on the other hand, are more prone to failure during rapid startup and can be larger making them more suitable for stationary applications (Hodjati-Pugh et al., 2021).

mT-SOFCs were originally developed because of the inverse relationship between the cells diameter and the power output per unit volume (Jamil et al., 2019). To provide structure to the cell, researchers have favored making the cells anode-supported because there are multiple downsides with making the other components the "backbone." Having an anode-supported cell is beneficial for fabrication, increased strength and great cell performance (T. Liu et al., 2015). Having an electrolyte supported cell increases the ohmic losses because of how thick the electrolyte becomes and the higher resistance to oxygen ion transport (Jamil et al., 2015, 2019; Lawlor et al., 2009). Additionally, when looking at both performance and cost, cathode supported cells are optimal based on performance while electrolyte supported cells are best when it comes to cost, however, anode supported

cells are the best balance of the parameters (Chelmehsara & Mahmoudimehr, 2018). To overcome the limitations of using an anode-supported mT-SOFCs, researchers have found that increasing the porosity of the anode has increased power output because there are less resistive pathways for the gas to travel through (Essaghouri et al., 2022; Jamil et al., 2019; Lawlor et al., 2009; Ormerod, 2003; Zhang et al., 2021). However, increasing the porosity decreases the structural integrity of the cell overall (Jamil et al., 2019). Another method to create a less resistive pathway is to decrease the thickness of the anode altogether allowing for higher mass transport. This is beneficial but previous research has shown that achieving this through the typical anode manufacturing techniques is costly and the extrusion process is so time consuming that it takes a while to be able to test whether any modifications will have an effect (M. Liu et al., 2011). Although there is a linear relationship between dipping the cell and how thick the anode gets, it is still lacking in the precision that can be achieved compared to a process such as extrusion (M. Liu et al., 2011; Zhang et al., 2021).

Electrochemical impedance spectroscopy (EIS) is a non-destructive method to uncomplicate physiochemical phenomena occuring in electrochemistry (Ciucci & Chen, 2015). The resistance is found at different frequencies and then through using equivalent circuit models, the resistances are related to different phenomena based off the frequency they are occuring at. The issue with this is there can be many different equivalent circuit models that have properties occuring at the same frequency (Sumi et al., 2020). Distribution of relaxation times (DRT) is a method for deconvoluting the electrochemical response of the system by using the premise that the responses of the system decay in relation to the systems timescale characteristics (Ciucci, 2019). DRT plots gamma, which is a transformation value that deconvolutes EIS data and is representative of how much of

a physiochemical process is occuring. DRT is a technique that has more recently been applied to SOFCs and there has not been a consensus on what each peak at various frequencies mean (Sumi et al., 2020).

As discussed, the amount of power produced by the fuel cell is dependent on how well the fuel and oxygen travel through the various layers of the cell. Few studies have explored the effects of varying the anode thickness of a mT-SOFC because more research are focusing solely on planer cells. By using different extrusion dyes, various anode thicknesses can be fabricated and the impact of the anode thickness on mass transport losses can be investigated. This study focuses on fabricating mT-SOFCs with different anode thicknesses to understand the correlation between anode thickness and power output, the way the resistance manifests itself in polarization losses and to determine what peak(s) in DRT are related to mass transport losses.

CHAPTER 2

LITERATURE REVIEW

The literature review for this master's thesis provides insight into the problem being addressed. The review begins with a background on SOFCs looking at how they work, their benefits and limitations, and what future work can be done to improve them. Following this, details on anode supported SOFCs are described and the pros and cons associated with this design are explained. Next, fuel cell mass transport will be explained including the methods of transport as well as their associated downfalls. Finally various methods for characterizing the fuel cells performance will be elaborated on including scanning electron microscopy (SEM), polarization curves, electrochemical impedance spectroscopy (EIS) and distribution of relaxation times (DRT).

Solid Oxide Fuel Cells (SOFCs)

Fuel cells are electrochemical devices that convert a fuel and oxidizer into electricity with minimal harmful byproducts. There comprised of the same 3 components that are in a battery: an anode, electrolyte, and cathode. The cell is fed hydrogen which is oxidized as it passes through the anode while, simultaneously, oxygen is reduced as it passes through the cathode. The global reaction occuring is:

$$H_2 + O^{2-} \rightarrow H_2O + 2e^-$$

The electrons are removed from the hydrogen and transferred to the oxygen by traveling through an external circuit which is what creates the electricity. The oxygen ions are able to travel through the electrolyte to react with the hydrogen and form water (Yamamoto, 2000). The electrons are forced to travel through the external circuit because

the electrolyte only allows oxide ions to pass through (O'Hayre et al., 2016). A schematic of this entire process and the SOFC structure can be seen in Figure 1 below.

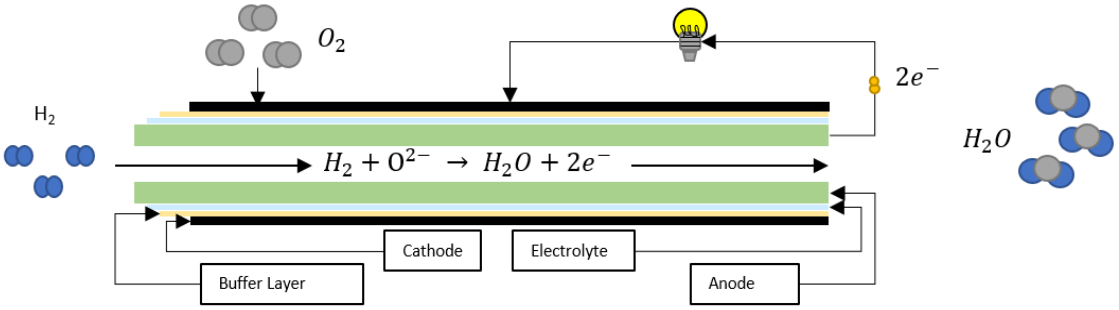

Figure 1: mT SOFC Schematic

Fuel cells are a promising solution for power generation because even the most efficient engine, the diesel engine, has an efficiency of 50% while currently fuel cells are able to reach an efficiency of 60% with the theoretical maximum being at 83% (Breeze, 2017). SOFC's differ from other fuel cells by having a ceramic electrolyte which requires them to operate at higher temperatures ranging from 600-1000°C (O'Hayre et al., 2016). Operating at these higher temperatures requires a higher power input during startup, but exothermic reactions maintain the high temperature at steady state. To minimize the losses associated with this, cogeneration systems have been created to harness the heat generated from operating at such high temperature and turn it into power (R. Milcarek et al., 2017; Ormerod, 2003). Cogeneration efforts are currently around 80-90% efficient making SOFCs higher operating temperatures more appealing (Riley et al., 2020). SOFCs benefit by operating at high temperatures because they are able to run on multiple different fuel sources (R. Milcarek et al., 2017; R. J. Milcarek & Ahn, 2019; Skabelund et al., 2020, 2022). Hydrogen is generally more costly to use as a fuel because it must either be reformed from hydrocarbons or generated via water splitting or electrolysis, so some cells instead

are run directly on hydrocarbons. Reforming hydrocarbons produces carbon dioxide which makes fuel cells a less clean energy conversion process (Breeze, 2017).

Operating at high temperature also creates another disadvantage in requiring materials that can withstand the high temperatures, operate reliably and alleviate thermal expansion coefficient mismatches (O'Hayre et al., 2016). The interconnects and external components of the SOFC also need to be able to withstand such high temperatures which is a significant increase in the cost of the system. Additionally, the high temperatures necessary for cell operation cause degradation and the cell to become unstable over time (Ivers-Tiffée et al., 2001). Fuel cells are only able to be used in high budget environments because of the high costs associated with manufacturing and they currently are not able to reach the power demand required for most portable or automotive applications, so a significant amount of work needs to be done to aid in their commercialization (O'Hayre et al., 2016) A commonly used cathode material is lanthanum strontium manganite (LSM) but when operating at intermediate temperatures (600-800°C), the LSM has decreased oxygen diffusion and electrocatalytic activity (R. J. Milcarek & Ahn, 2021). Researchers have started to use perovskites such as lanthanum strontium cobalt ferrite (LSCF) as a cathode material because they are able to meet the shortcomings that LSM has in intermediate temperature ranges (R. J. Milcarek, Wang, et al., 2016). Perovskites, however, are incompatible with the YSZ electrolyte because when the two materials come in contact, they react to produce different materials such as $La_2Zr_2O_7$ or $SrZrO_3$ which are significant hinderances to the performance because they are non-conductive. To prevent the two materials from reacting a buffer layer material is added usually made of doped-ceria, such

as samarium doped ceria (SDC), because it is chemically compatible with the LSCF (R. J. Milcarek & Ahn, 2021).

Anode-supported mT-SOFC

In a mT-SOFC, many of the layers are brittle so one of the layers thicknesses is significantly increased compared to the others to provide structure. The anode, electrolyte and cathode all can be used to support the cell but the performance of the cell is better if it is supported at either electrode (Chelmehsara & Mahmoudimehr, 2018). Anode-supported cells have been considered favorable because they are able to operate at lower temperatures which allows for higher performance (Tseronis et al., 2008). One of the issues with choosing an anode-supported cell is that having a thicker anode increases the resistance for fuel mass transport. Although the resistance is an issue with this type of support, the anode is typically supplied with up to 100% fuel concentration while the cathode is being supplied with air where only ~21% of that is oxygen (O'Hayre et al., 2016). Even though it will hinder the performance somewhat, the effects are generally less than what would be produced from having a cathode supported cell (O'Hayre et al., 2016).

Fuel Cell Mass Transport

Mass transport pertains to how the reactants and products move within a fuel cell. This fuel cell process affects the performance in two ways, ensuring that enough fuel is being provided to the cell as well as ensuring the products are being removed from the cell at equal rates to prevent starving or strangling the cell (O'Hayre et al., 2016). There are two ways that the fuel can transfer through the electrode: diffusion, and convection. Convection is the term used to describe when the fuel is forced into the cell due to pressure

differences resulting in flow along the face of the anode in the case of a mT-SOFC. The way to increase mass transport through convection is to find the optimal rate at which to flow the fuel to the cell using the properties of the fluid and the dimensions of the cell (O'Hayre et al., 2016). Diffusion is the term used to describe a flow that occurs because of a concentration gradient. On the inside of the tube, the concentration gradient is formed because of the frictional forces created at the inner wall of the anode where the velocity at that point approaches zero. If the flow rate is high enough, however, then the pressure difference allows for convective mixing that prevents the concentration gradient from forming. Within the anode, concentration gradients can occur from a significant consumption of H_2 depleting it from the reaction site. This absence of H_2 is the driving force for diffusion processes in the region between the electrode and the reaction zone (O'Hayre et al., 2016). Concentration overpotential refers to when there is not enough fuel or oxidizer at either electrode to sustain the electrochemical reactions. While it is possible for this to occur at both the anode and cathode electrode, concentration overpotential at the anode leads to a more significant decrease in the voltage of the cell (Tseronis et al., 2008). Concentration overpotential is often an issue in anode-supported cells because it is directly correlated with the thickness of the anode because the reactants need to travel through that layer to reach the electrolyte.

Scanning Electron Microscopy (SEM)

To study the structure of a SOFC at the microscopic level, an SEM can be used to create images of the sample's crystalline structure and topography of the surface. After coating the sample with a metal, electrons are accelerated at high speeds in the microscope

in order to interact with the coating and provide information to the various detectors (Parry V, 2000). Some errors in performance pertain to manufacturing errors such as a non-uniform electrolyte or buffer layer (Nguyen et al., 2016). Looking at the cell on the microscopic level will allow for the nonuniformity to be identified.

Energy-dispersive x-ray spectroscopy (EDS/EDX) is a technique used to identify the elements present in the nanostructure of samples. EDS involves a focused probe that sends an electron beam and measures the resulting x-ray emission spectrum at different points along the sample and uses that spectrum to identify what elements are present (Alfonso et al., 2010). No elements have the same x-ray emission spectrum making it possible to distinguish the elements concentrations (Mutalib et al., 2017).

Polarization Curves

A polarization curve is generated with the current voltage method and can be used to display the performance of cells. As the current density is incrementally increased, the voltage is measured. The power density is then calculated by multiplying the current density by the voltage. The cell experiences activation, mass transport, and ohmic losses at the various current densities and by plotting the power density and voltage, the optimal conditions can be found. Activation losses pertain to the cells inability to overcome a certain barrier that would allow the process of turning reactants into products to begin (O'Hayre et al., 2016). Ohmic losses are associated with electrons inability to flow through the electrodes or the ions inability to flow through the electrolyte (T. S. Zhao & Xu, 2009). The final losses are associated with mass transport which will be discussed in the section below. The first portion of losses in voltage pertain to the activation region, the middle

portion pertains to losses in the ohmic region, and the last third pertains to losses in the mass transport region (O'Hayre et al., 2016).

To compare different fuel cells performance, at a chosen voltage the associated current density and power density are found on each graph (Bharti & Natarajan, 2022). The amount of power and current that can be produced is dependent on the active area of the cell, so the graphs are plotted in power and current density to allow for the results to be comparable (O'Hayre et al., 2016).

Electrochemical Impedance Spectroscopy (EIS)

EIS is a technique used to study key physical properties in most electrochemical applications that is easy to implement, very accurate, and provides information at a variety of different frequencies(J. Liu et al., 2020). A sinusoidal current or voltage is used to perturb the system and the resulting voltage or current, respectively is measured. The difference in amplitude between the voltage and current as well as the phase lag are then used to obtain the impedance (R. J. Milcarek & Ahn, 2019). Although the results can be difficult to interpret, EIS data can help distinguish ohmic, activation, and concentration losses in an electrochemical system (O'Hayre et al., 2016). There are three conditions that the tests need to meet in order for the data to be useful: the system needs to be stable, there needs to be perturbation linearity, and the measured current or voltage must be solely caused by the applied voltage or current (R. J. Milcarek & Ahn, 2019). To be able to interpret the electrochemical data, equivalent circuit models have been created where most of the aspects of the system are kept the same except for one of the components that is varied (Hsieh et al., 2015). Tests are run with the specific component being varied and the

results are studied to determine how the parameter influences the impedance at each frequency. These results can be difficult to interpret because the data can be fitted to different models, so it is not easy to precisely predict what frequency corresponds to that component of the circuit. There are analytical models made for porous materials that allow for more accurate results because they require less unknowns to make conclusions and at a variety of frequencies, the results from the model are closer to the actual results of the system (R. J. Milcarek & Ahn, 2019). The EIS data can be graphed in two forms, a Nyquist plot and a Bode plot. The Nyquist plot involves graphing the real impedance on the x-axis and the imaginary impedance on the y-axis. The point at which the data crosses the real axis as well as the curvature of the semi circles peaks in the positive region of the imaginary axis tell information about the ohmic, anode activation, and cathode activation losses. The bode plot involves graphing the frequency on the x-axis and the imaginary component of the impedance on the y-axis. Using both the Bode and the Nyquist plot, the frequency at which the data crosses the imaginary axis can be identified.

By measuring the EIS for SOFCs with different anode thicknesses, the effects on the resistance of the cell can be observed. Changes observed in the low frequency range can be related to the diffusion process at the anode interface while changes in the high frequency range can be related to the activation polarization at the cathode, but the results can differ depending on the cell configuration (Hsieh et al., 2015). The slowest process for anode-supported mT-SOFCs is anode diffusion because of the how much thicker the anode layer is in comparison to the electrolyte and cathode. This suggests that the lower frequency ranges correspond to the slower processes and the higher frequency ranges correspond to the faster processes (Tian & Milcarek, 2022).

Distribution of Relaxation Times (DRT)

DRT is a method of analyzing EIS data that assumes the electrochemical response of the system follows a distribution of relaxations (Ciucci & Chen, 2015). By this, it means that it uses the time scale and its characteristics to find out information about the circuit instead of trying to fit it to an equivalent circuit. The premise is that if the system is perturbed with a current or voltage, the responding voltage or current will be decreased for a specific time. DRT has been used in the past for evaluating polarization resistances between cells with different anode materials as well as understanding the internal reforming of hydrocarbons being used as fuel for SOFCs. Previous studies have looked at which peaks at various frequencies correspond to different physiochemical origins occuring in the cell (Caliandro et al., 2019; Hong et al., 2020; Sumi et al., 2020). In Table 1, this is what an anode-supported mT- SOFC has found each peak to relate to (Sumi et al., 2020). However, the exact results can vary depending on the cell structure and materials as reported in previous studies (R. J. Milcarek & Ahn, 2018; Tian & Milcarek, 2022).

Table 1: Physicochemical DRT Peaks for Anode-Supported mT-SOFC (Sumi et al., 2020)

Frequency	Electrode	Physiochemical Origin
10 – 100 kHz	Cathode	Ionic conduction process in the mixed ionic-electronic conductor
0.1 – 10 kHz	Anode	Charge transfer and ionic conduction processes

20 – 1000 Hz	Anode	
2 – 200 Hz	Cathode	Oxygen surface exchange and diffusion processes
0.5 – 20 Hz	Anode	Gas diffusion process in the anode substrate for anode-supported cells
0.05 – 1 Hz	Anode	Oxygen nonstoichiometric variation process at the interface between YSZ electrolyte and Ni-GDC anode co-sintered at high temperature

CHAPTER 3

FUEL CELL FABRICATION

Ni-YSZ SOFC Fabrication

Anode supported SOFCs were fabricated using techniques reported in previous papers (R. J. Milcarek et al., 2019; R. J. Milcarek & Ahn, 2018, 2021). In addition, experimentation was done to find the sintering temperature for the electrolyte that ensures the buffer layer could be dipped onto the cells while preventing interfacial reactions (T. S. Zhao & Xu, 2009).

Anode Fabrication

The anode was fabricated using a mix of nickel oxide (NiO, Fuelcellmaterials) and yttria-stabilized zirconia (YSZ, Tosoh) using 60% NiO, 4% YSZ – 8Y, and 36% YSZ - 8YS. This was combined with methocel, MX-1000, steric acid, water, and polyethylene Glycol (PEG)-1000. After these were all combined, they were put through an extruder and different dyes were used to create 6 different inner diameters: 2.896mm, 2.997mm, 3.099mm, 3.200mm, 3.302mm, and 3.404mm.These cells were placed in trays to dry for 1 week. Then they were cut and prefired to 1100°C.

Electrolyte Fabrication

The electrolyte was made using YSZ – 8Y powder combined with polyvinyl butyral (PVB), phosphate ester (PhE), and PEG – 100. The mixture was ball milled for 2 hours at a speed of 4 then dipped onto the cells using a dip coating machine (MTI Corporation). The goal was to fire the cells at a temperature that would allow for the buffer layer to be

dipped on so three cells were fired at 1350°C, 1375°C and 1400°C. The cells were then dipped with the buffer layer and cathode and then they were taken to the SEM where the various layers thicknesses were measured. The best thickness was found at an electrolyte firing temperature of 1375°C so the remaining cells were fired at this.

Buffer Layer Fabrication

The buffer layer was made using samarium doped ceria (SDC) -HP powder combined with PVB, 1-methoxy-2-propanol (1M2P), PhE, and PEG – 100. This mixture was ball milled for 2 hours on a speed of 4, then the cells were dipped into the slurry twice, being placed into an oven at 130°C after each layer until dry. Following this, the cells were fired at 1200°C.

Cathode Fabrication

Finally, the cathode was made using lanthanum strontium cobalt ferrite (LSCF) -HP powder and SDC-HP powder combined with PVB, 1M2P, PhE, and PEG – 100. The ratio of LSCF to SDC was 7:3.th This mixture was ball milled for 2 hours on a speed of 4, then the cells were dipped into the slurry twice, being placed into an oven after each dip to dry at 130°C until dry. Following this, the cells were fired at 1100°C.

Fabrication Failures

While firing the cells, it was noted that the furnace does not reach a uniform temperature throughout. Temperature measuring ceramics were placed throughout the chamber and the temperature varied between 10-25 °C. The cells, depending on their location may have not reached the correct sintering temperature causing issues within the

microstructure of the cell's layers. Images were taken with the SEM post testing to observe what the effects of the nonuniform temperature were.

CHAPTER 4

EXPERIMENTAL SETUP

The purpose of this experiment is to test for changes in performance due to decreasing the thickness of the anode. To test this, only H_2 gas was used as a fuel source. Shown below in Figure 2 is the experimental setup.

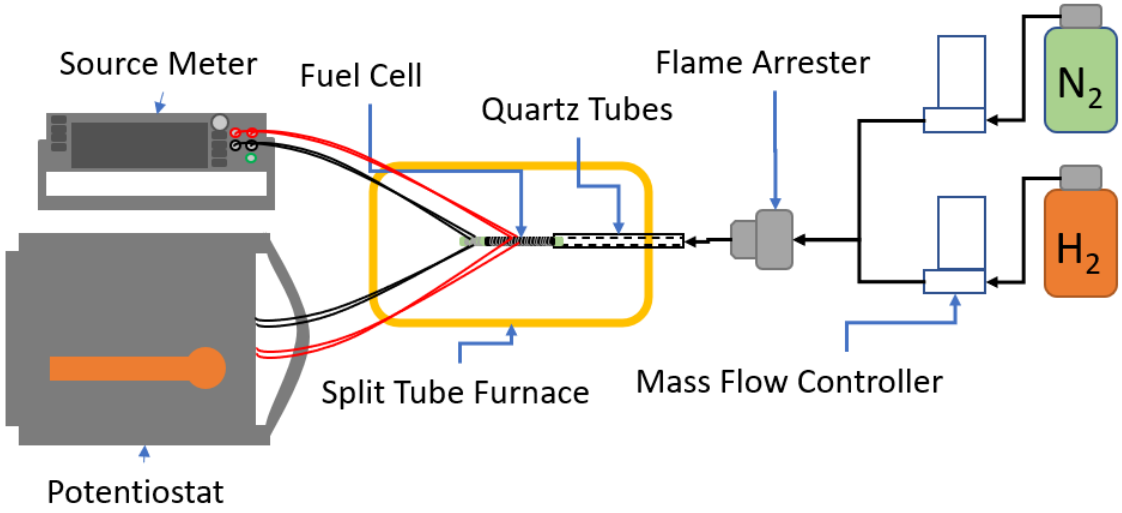

Figure 2: Experimental Setup

The fuel cells anode and cathode were painted with silver paste to act as a current collector. The exposed portion of the anode was painted while the 4 cm active area of the cathode was painted. Two wires were created, one consisting of a silver and steel wire wrapped together, the other consisting of a three silver wires wrapped together. Then, these two wires were attached to each electrode by wrapping them with silver wire. The anode portion was additionally covered in ceramabond to prevent any gas leaking. The fuel cells were then sealed to a quartz tube using ceramabond as well to prevent any leaking. The ceramabond was air dried for 4 hours prior to any heating. This setup was placed inside a split tube furnace where it was heated up to 750°C over the course of 200 minutes. After

reaching the temperature the cell was held there for 10 minutes after which it was supplied N_2 and H_2 each at a rate of 30 mL/min to reduce the NiO to Ni in the anode. The cell reduced for 3 hours while the OCV was measured every 1 second using the I-V (current-voltage) method with the 4-probe technique. After reduction was complete, the experiments were run as follows.

1) The cell was supplied only H_2 at 4 rates of 10, 20, 30, and 40 mL/min where the power density, current density and voltage were measured ending at a cut off voltage of 0.4 V. The cell started with 40 mL/min and the flow rate was swept down to 10 mL/min before going back up, therefore having tested at each flow rate twice.
2) An Electron Impedance Analyzer was attached to the cell to test the EIS of the cells. The EIS test was run for each cell 3 times at each flow rate.
3) Finally, the polarization curves were run again but this time at a cut off voltage of 0.2 V. This was done after the EIS to prevent skewed data that could have occurred due to the deterioration caused by running down to such a low voltage.

CHAPTER 5

RESULTS

Very few studies look at how decreasing the anode thickness increases the fuel cell mass transport in mT-SOFCs. To accomplish this, fuel cells have been fabricated by extruding various anode thicknesses and dip coating an electrolyte, buffer layer, and cathode onto the cells. Six different anode thicknesses were fabricated but only the largest and smallest anode thicknesses were tested to find differences in the performance of the cells. First, they were supplied equal amounts of hydrogen and nitrogen for 3 hours to reduce the cell. Then to test the performance of the cell, polarization curves and EIS were run at 4 different flow rates. The polarization curves were taken first with a cut off voltage of 0.4 V and then again after the EIS data had been taken, this time with a cut off voltage of 0.2 V. DRT was conducted on the EIS data to deconvolute it and determine the various phenomenon occuring during testing. Finally, the samples were taken to an SEM where images were taken of the cross sections and EDX scans were conducted. Uncertainty analysis was conducted on 3 tests of each cell thickness and error bars were presented on the Nyquist plots.

SEM

In Figures 3 and 4, a cross section can be seen at two points for the same cell. Between the two images, the thickness on the anode varies depending on which area you look at showing that there is a lack of uniformity created during the extrusion process. The thickness of the anode was measured at multiple different points to observe if there are any discrepancies in the anode thickness values and were placed in table 2 below. Based off

the dyes used during anode extrusion, the thick anode cell should be ~254 µm thicker than the other layers, however, the average thicknesses were only turning out to be 50 µm different. The anode thicknesses measured were ranging between 200-300 µm for cells of the same thickness, alluding to errors in the manufacturing process creating a non-uniform anode all around. The lack of uniformity creates a less resistive pathway for the fuel to travel at some points and likely causes concentration overpotential to occur non-uniformly. This could directly have affected the performance of the cell and explain any lower power density.

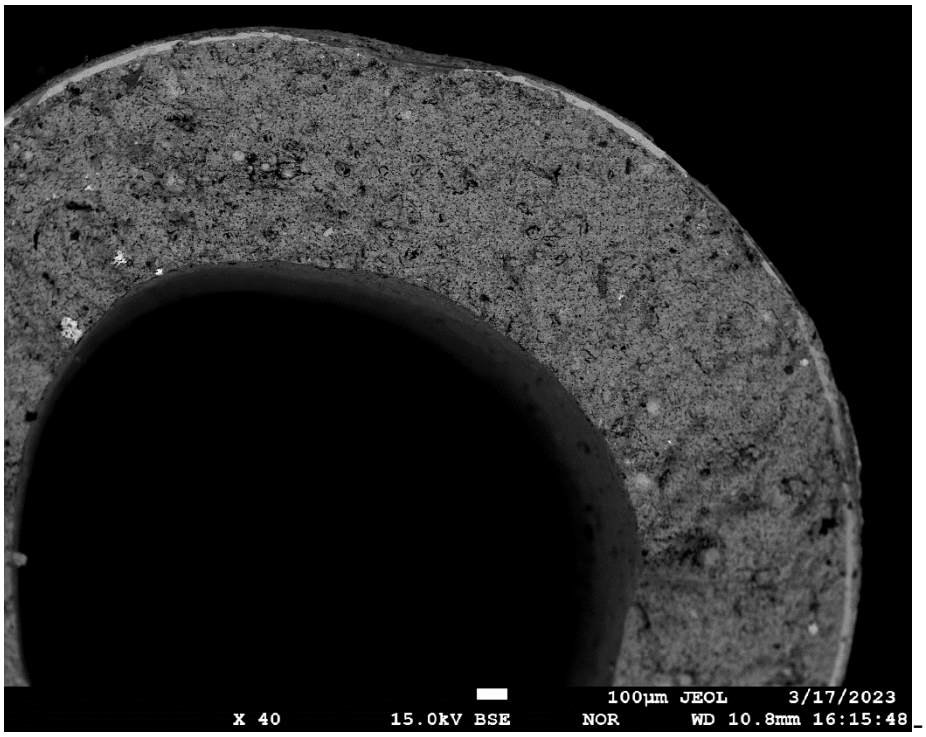

Figure 3: Thick (620µm) Inner Diameter Anode Cross Section Top

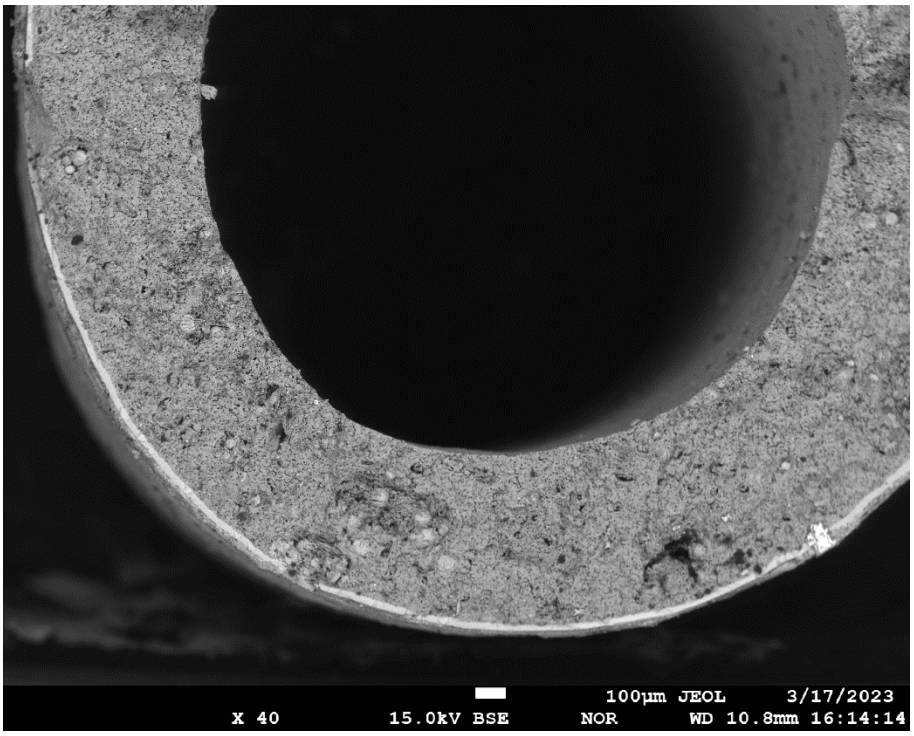

Figure 4: Thick (620µm) Inner Diameter Anode Cross Section Bottom

Table 2: Average thicknesses of the layers for thick and thin cells using SEM (in µm)

	Thin (3.404mm)	Thick (2.896mm)
Anode	575 ± 119	620 ± 100
Electrolyte	15.5 ± 1.2	20.9 ± 3.4
Buffer Layer	12.5 ± 3.6	12.3 ± 6.2
Cathode	19.5 ± 3.7	14.9 ± 5.6

Figure 5 is an EDS test scanned from the cathode into the electrolyte to determine which elements are present. Using Table 2 and examining Figures 3 and 4, the 11.05-23.35 µm range in figure 5 should pertain to the buffer layer. In the graphs, there is overlap

between the YSZ electrolyte and LSCF cathode. The buffer layer is put in place because if the electrolyte and cathode react, it creates a compound that leads to an increase in the ohmic resistance, hindering the performance of the cell (Uchida et al., 1999). There is a clear presence of both the cathode and electrolyte materials in the region that should be the buffer layer suggesting that the electrolyte and cathode reacted with each other. Overlap implies that the performance of the cell will be lower than expected because of an increased resistance from the material formed by the electrolyte and cathode reaction (R. J. Milcarek, Wang, et al., 2016).

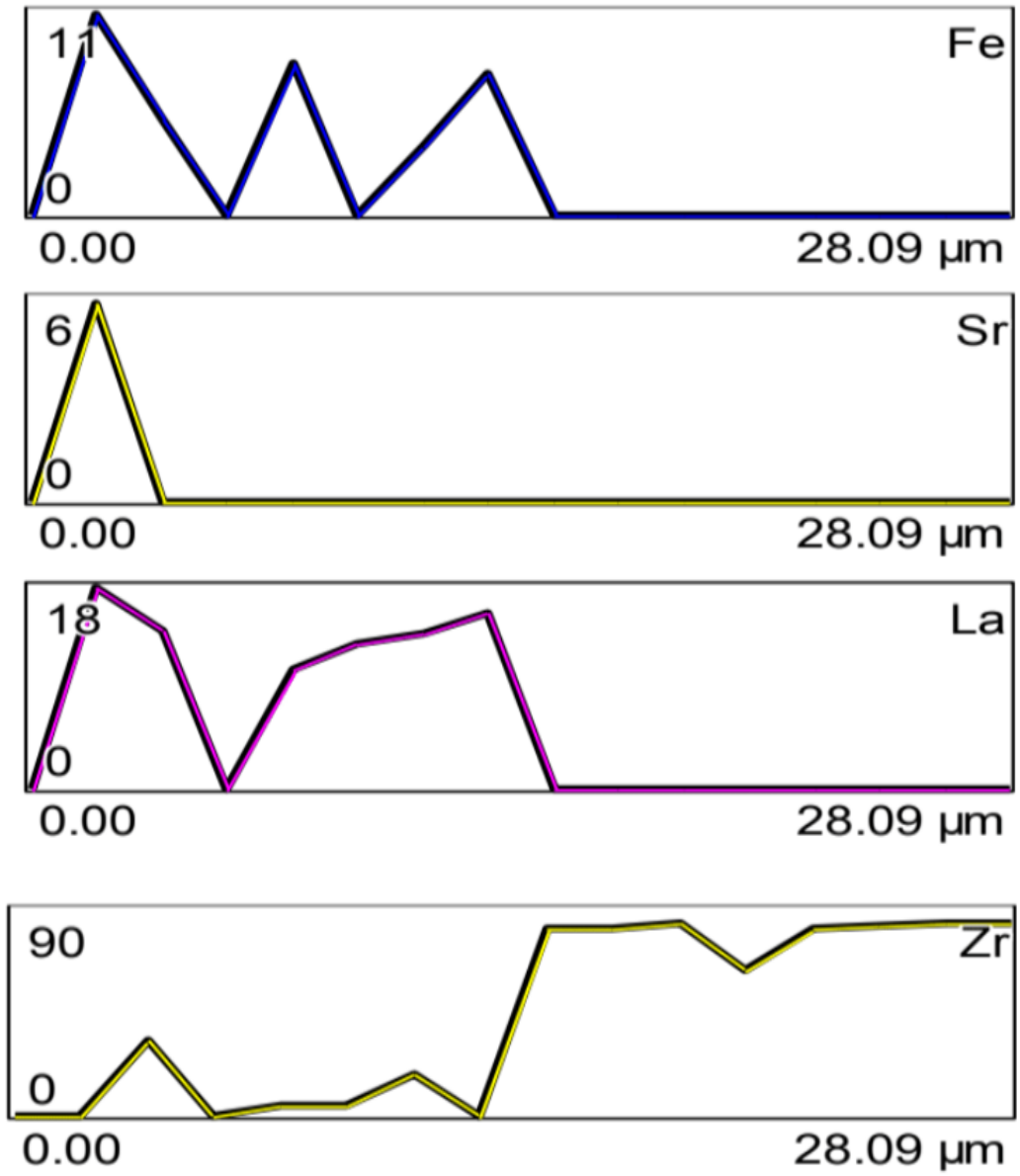

Figure 5: EDS Test for thick (620µm) Anode Inner Cell Diameter

Reduction

The open circuit voltage (OCV) was measured for the cell as soon as the hydrogen and nitrogen started flowing through the cell which can be seen below in Figure 6. The OCV was measured every second and during each test there was a point where the cells OCV jumped from around 0.3 to 0.9 V. This jump occurs earlier for the cells with a thinner

anode, suggesting that the gasses were able to diffuse through the anode layer faster and reduce the NiO to Ni at a noticeably faster rate. Looking at the first 1000 seconds in Figure 7 the difference in time taken to make the jump is only about 80 seconds meaning it jumps up only 1 minute faster. Although this is a noticeable difference, it is not a significant one because both cells are able to achieve similar power densities. The SEM results reveal that on average the anode thickness only differed by around 50 µm between the thick and thin anode cells. The small difference in thicknesses explains why the difference in reduction time was so insignificant, because reduction is directly dependent on the anode thickness. To reduce the NiO to Ni, H_2 needs to diffuse through and react with the anode layer.

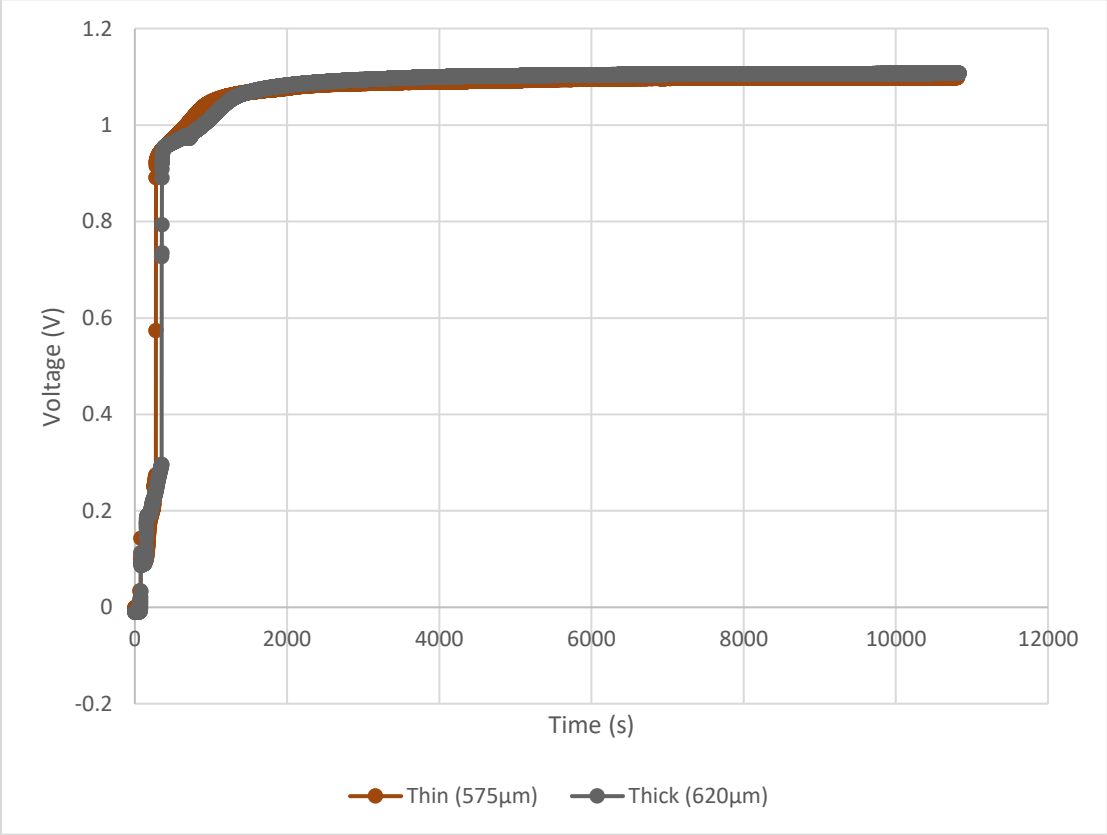

Figure 6: Reduction of cells at 750°C for 3 hours flowing 30mL/min each of H_2 and N_2

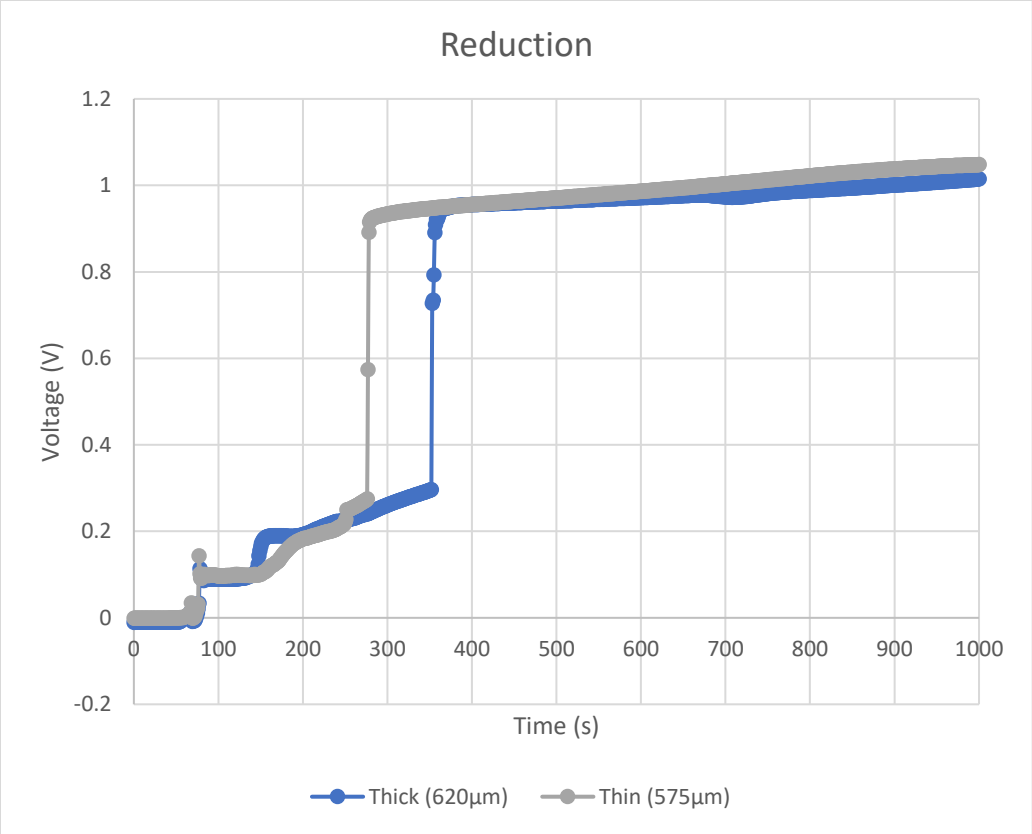

Figure 7 : First 1000 Seconds of Reduction from Figure 6

Polarization Curves

The polarization curves for one of the thickest and one of the thinnest anode cells at a flow rates of 10mL/min, 20mL/min, 30mL/min, and 40mL/min are shown below in Figures 8-11. There is no significant difference in the power density achieved for the different anode thicknesses but in general the thinner anodes did have a slightly higher power density as shown. As can be seen from the SEM results, there is evidence that the cathode material leaked through the buffer layer onto the YSZ forming a resistive layer suggesting that a higher power density could have been achieved (R. J. Milcarek, Wang, et al., 2016; Uchida et al., 1999). These curves were run twice with a cut off voltage of 0.2 V, which at this low of a voltage can damage the cell. At higher current densities, the

decrease in voltage has to do with mass transport losses and for all of the flow rates seen in Figure 8-11, the region of the graph where curves start to significantly deviate for the thicker and thinner anode are all at higher current density values. This shows that the there are higher mass transport losses between the thicker and thinner cell which is to be expected because reducing the anode thickness creates a less resistive pathway for the gas to diffuse through. In the ohmic region, losses can occur here due to resistance preventing oxide ions from passing through the electrolyte (Mohammed et al., 2019). From the SEM images, there is a 33% increase in the thickness of the electrolyte for the thicker cells so at increased flow rates, it becomes a barrier slowing the reaction from occuring. The graphs do not deviate significantly in the lower frequency range pertaining to activation losses. Changes to losses here can be made here by increasing the temperature of the system or increasing the amount of reactants at the reaction site (O'Hayre et al., 2016). However, changes to the concentration of the reactants will be more prevalently seen in the mass transport losses and there was no change to the operating temperature explaining why the voltage dropped at the same rate for both the thick and thin cells in the activation losses region of the polarization curve.

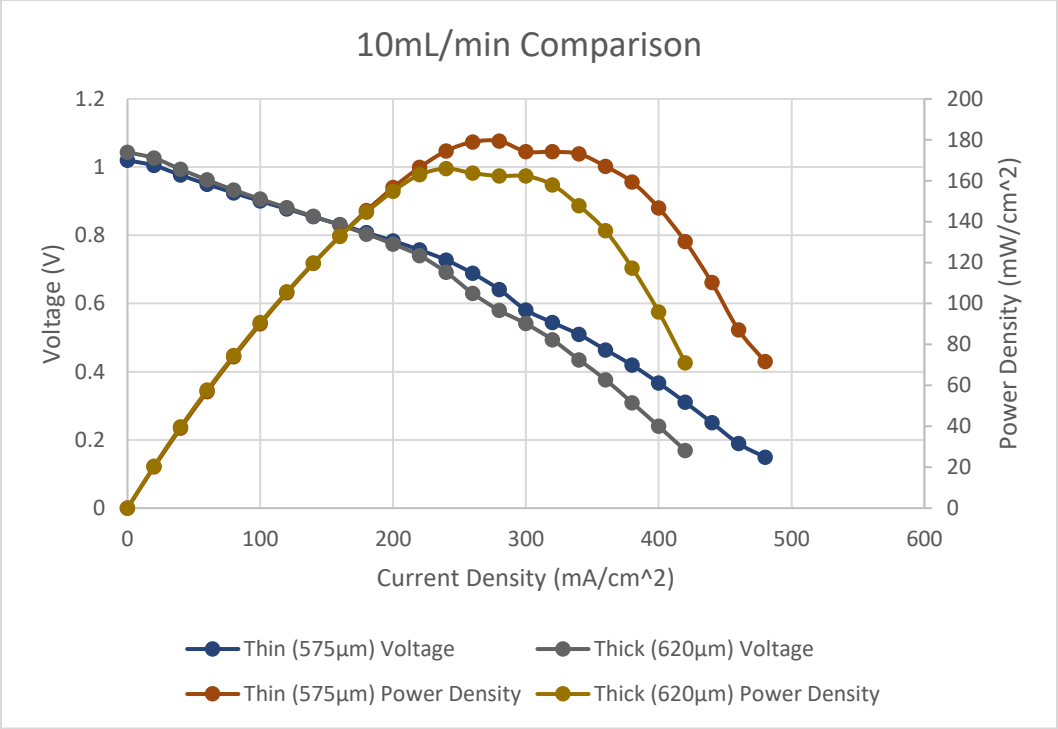

Figure 8: Polarization curves at 10mL/min H_2 at 750°C for Thick and Thin Cells

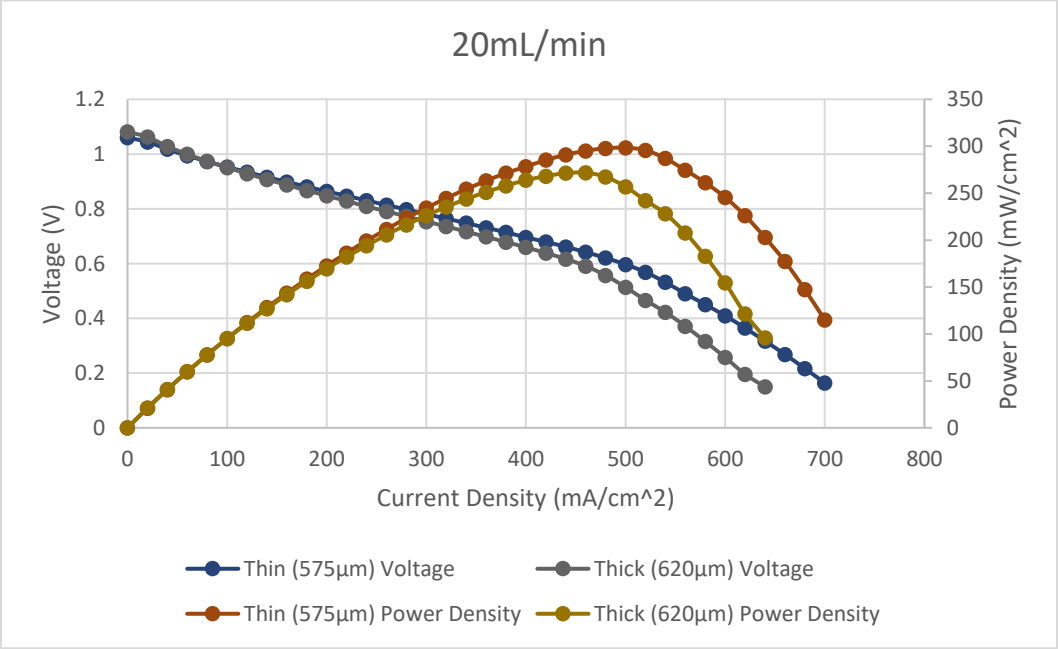

Figure 9: Polarization curves at 20mL/min H_2 at 750°C for Thick and Thin Cells

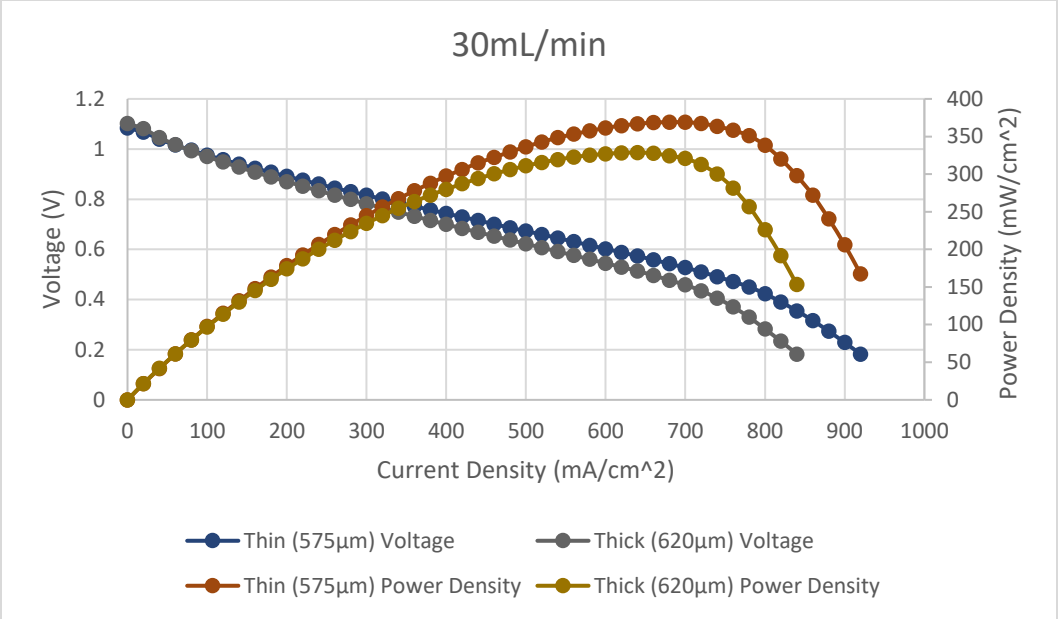

Figure 10: Polarization curves at 30mL/min H_2 at 750°C for Thick and Thin Cells

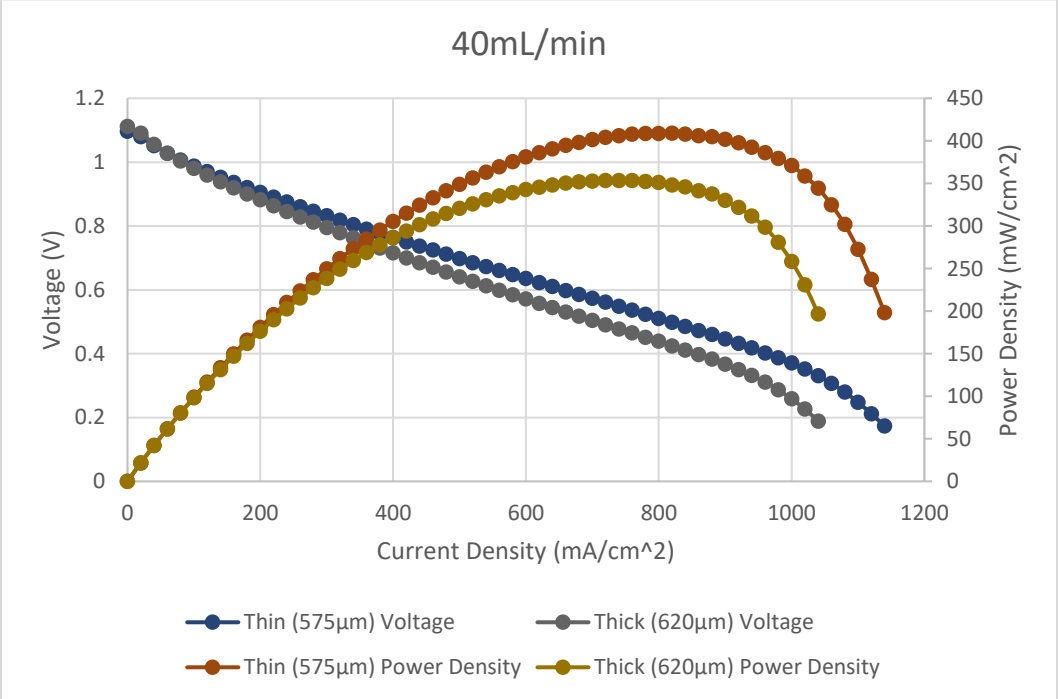

Figure 11: Polarization curves at 40mL/min H_2 at 750°C for Thick and Thin Cells

EIS

Below are the Nyquist plots for the thick and thin cells at all four of the flow rates in Figures 12-15. All of the graphs cross over the real axis at a high frequency making the point at which they cross over representative of the ohmic loss (O'Hayre et al., 2016). The thinner cells cross over at lower impedance values than the thicker cells meaning that there is less ohmic resistance. By thinning the anode layer, the electrons had a shorter pathway to transfer through to get through this layer and to the external circuit. At the lower flow rates, there is a smaller difference between the points at which the graphs are crossing the real axis which makes sense because having a lower flow rate there could be insufficient reactants reaching the reaction site. Additionally, the results from the SEM suggest that the ohmic resistance is higher than expected because of the potential reaction occuring between the YSZ and LSCF, therefore, this is not representative of the full potential the cells have (R. J. Milcarek & Ahn, 2021).

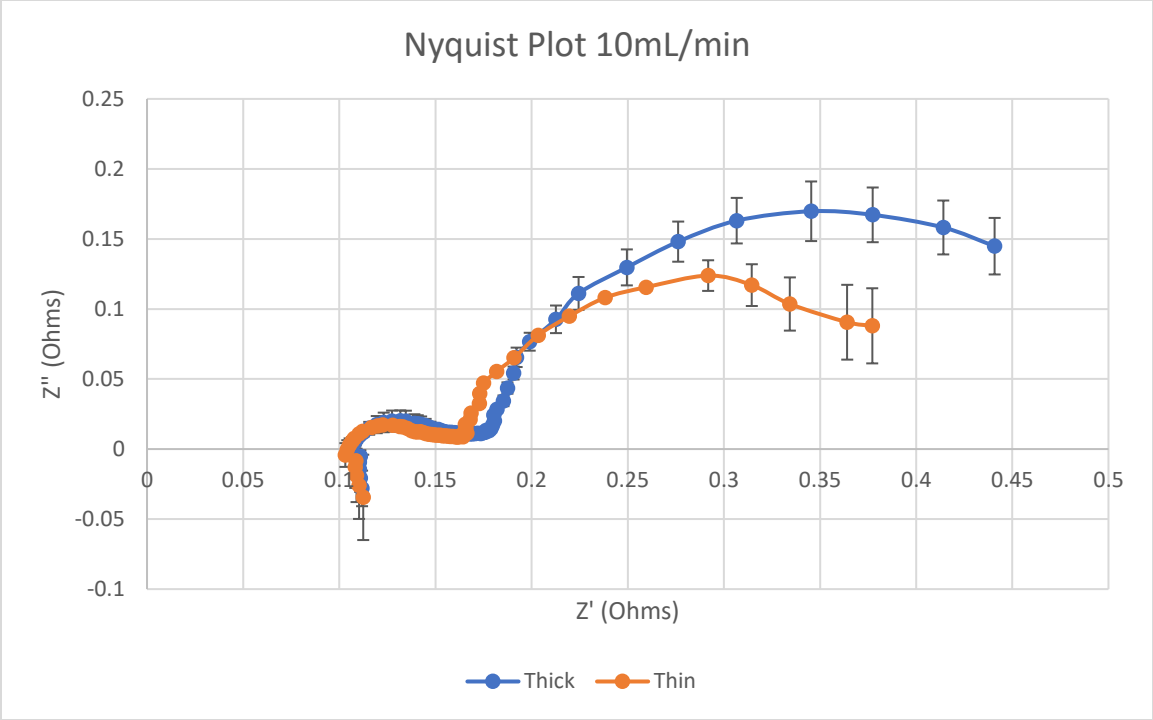

Figure 12: Nyquist Plot at 10mL/min H_2 at 750°C for Thick and Thin Cells

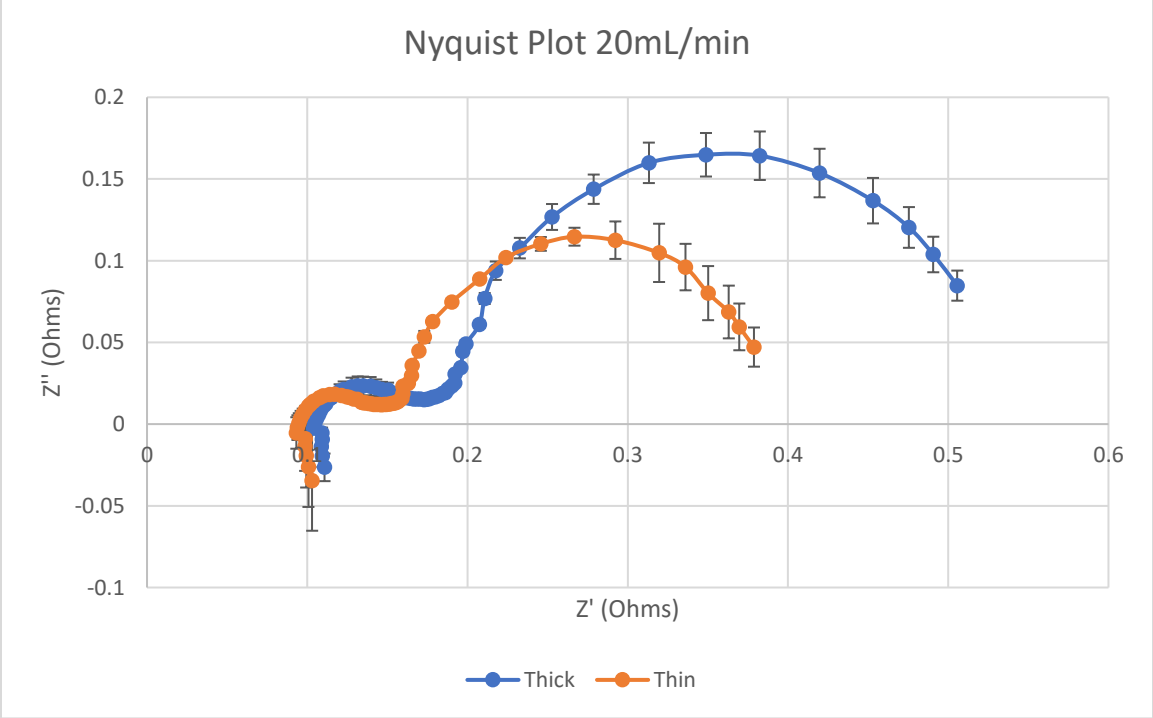

Figure 13: Nyquist Plot at 20mL/min H2 at 750°C for Thick and Thin Cells

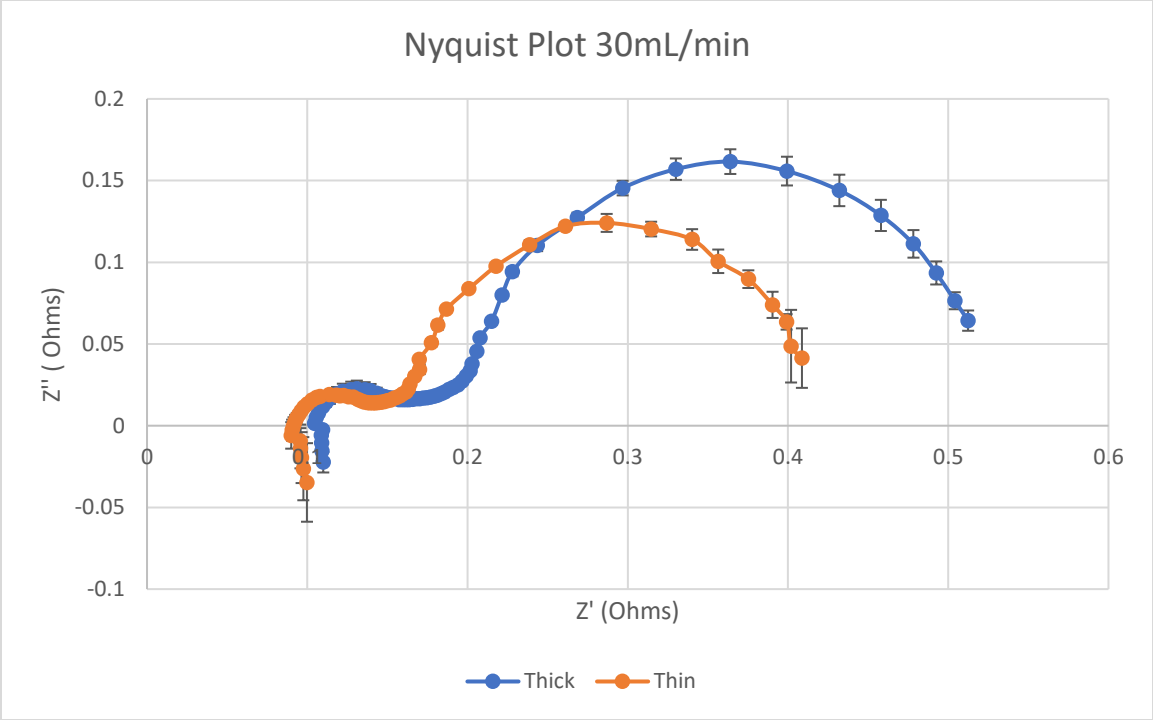

Figure 14: Nyquist Plot at 30mL/min H_2 at 750°C for Thick and Thin Cells

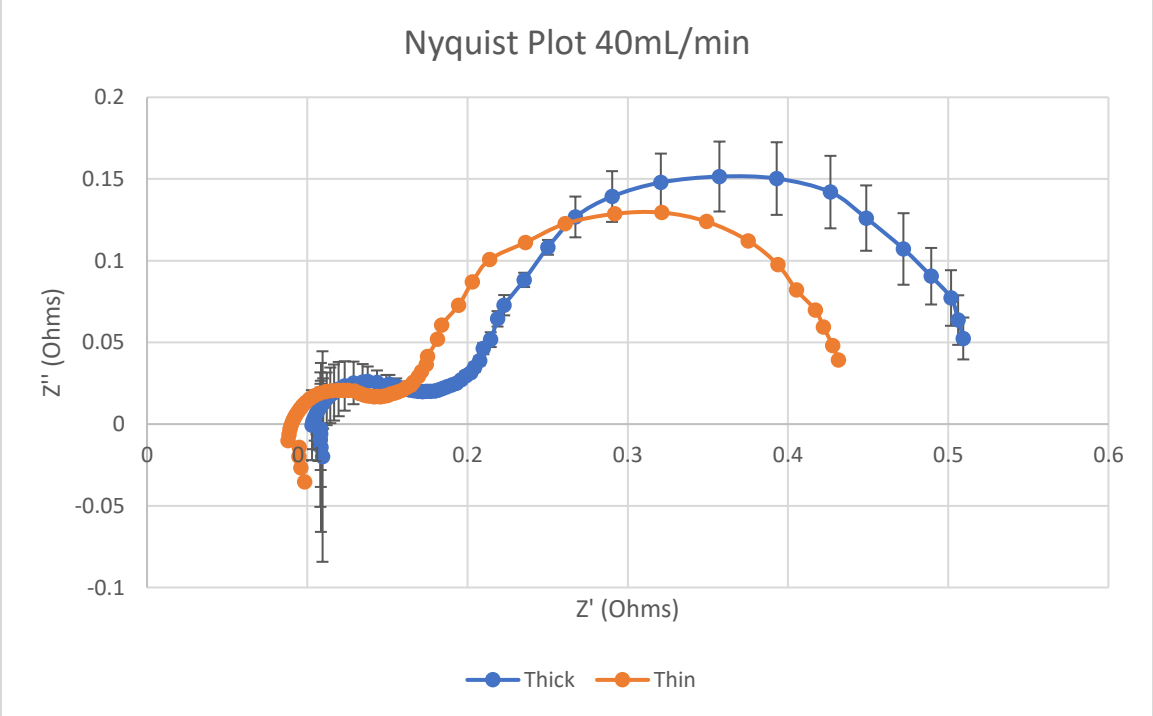

Figure 15: Nyquist Plot at 40mL/min H_2 at 750°C for Thick and Thin Cells

Below in Figures 16-19 are the Bode plots of the EIS data. At lower frequencies, the resistance varies between the cells and differences in this frequency range suggests that there is a difference in the diffusion process at the anode surface (Hsieh et al., 2015). Mass transport losses have been observed with similar mT-SOFCs at this frequency range (R. J. Milcarek, Garrett, & Ahn, 2016). The differences in the diffusion process suggests that more of the reactants can reach the reaction site for the thinner cell than that of the thicker preventing or mitigating the effects of concentration overpotential. The difference in impedance is largest for the lowest flow rate and smallest for the highest flow rates. Mass transport losses increase for lower flow rates because there are not enough reactants being supplied to the reaction site, further confirming that the lower frequencies pertain to this process. There is variation of impedance at higher frequencies and any variations in this frequency range suggest that there are differences in the ohmic resistance (Chang et al., 2019). The value of impedance differs the most at higher frequencies for the highest flow rate meaning the two cells running at 40mL/min have the largest difference in ohmic resistance. The ohmic resistance pertains to the ability for electrons and ions to be transported and because of the increased flow rates, there is enough reactants being supplied so the electrons encountering resistance when traveling through the anode is what causes the most losses (O'Hayre et al., 2016). The ohmic resistance being largest for the

highest flow rate reinforces the conclusions drawn from the polarization curves.

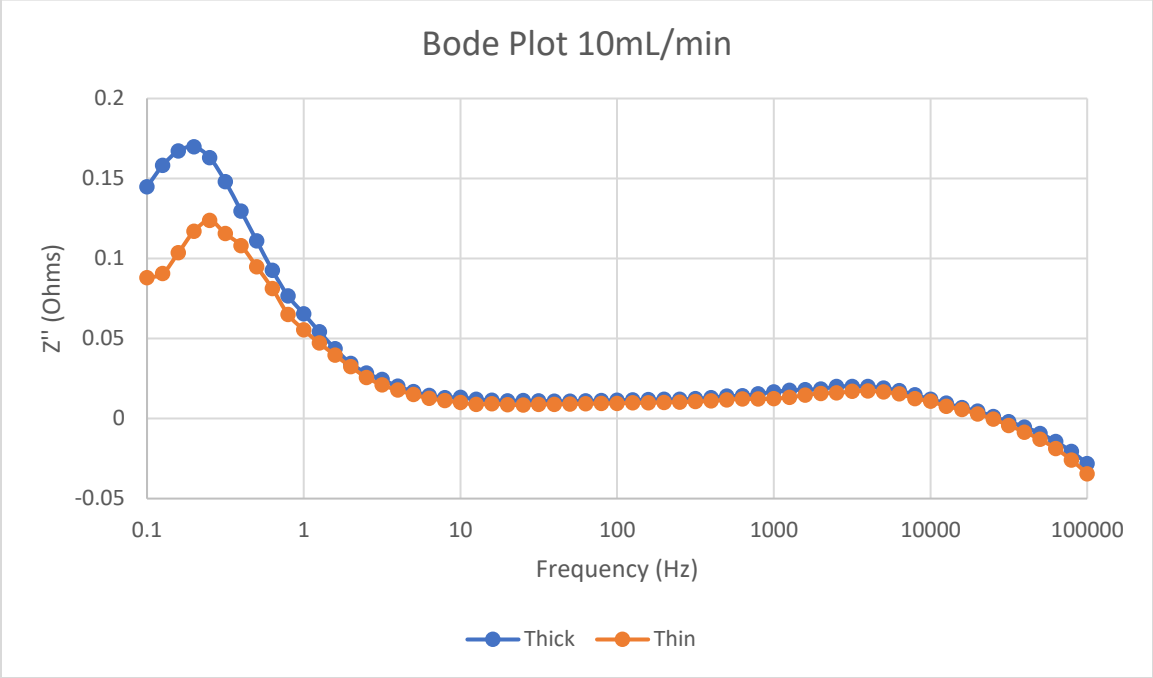

Figure 16: Bode Plot at 10mL/min H_2 at 750°C for Thick and Thin Cells

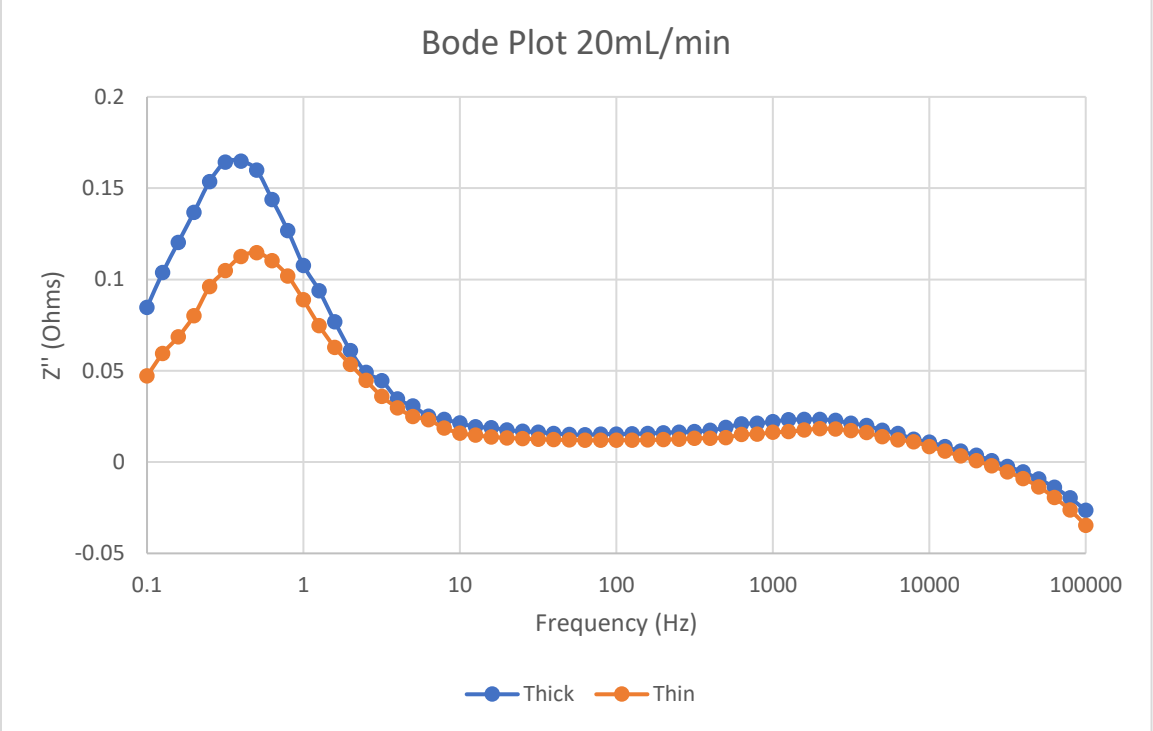

Figure 17: Bode Plot at 20mL/min H_2 at 750°C for Thick and Thin Cells

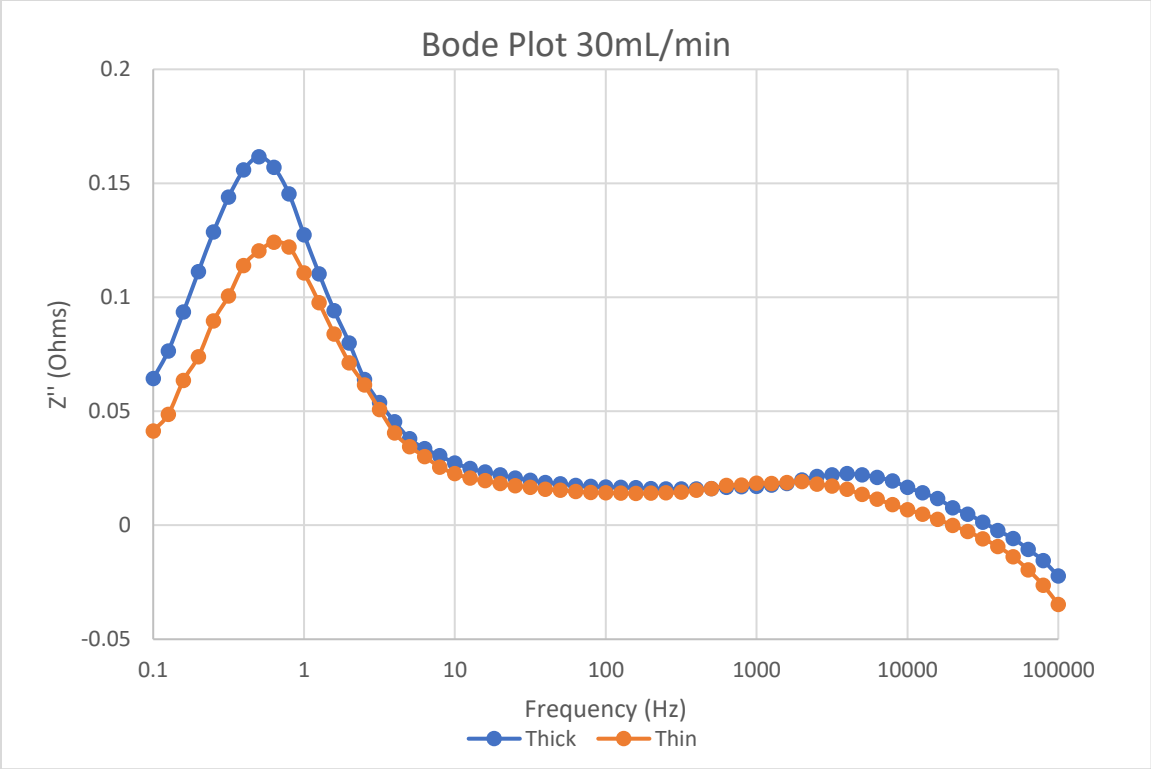

Figure 18: Bode Plot at 30mL/min H_2 at 750°C for Thick and Thin Cells

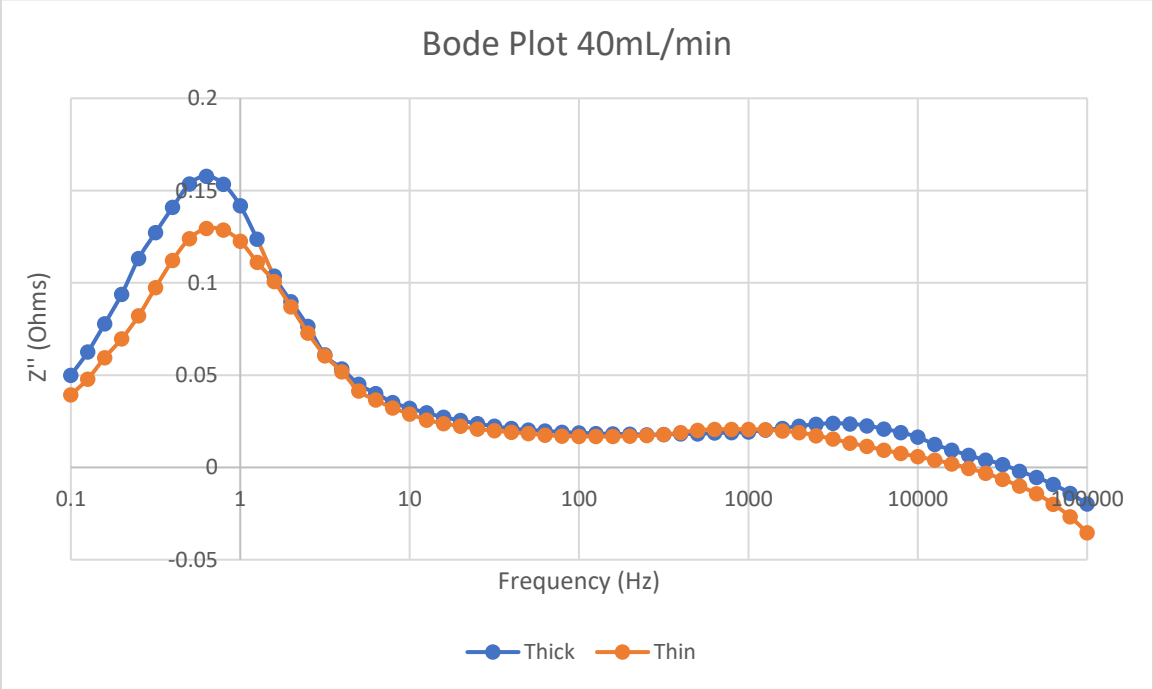

Figure 19: Bode Plot at 40mL/min H_2 at 750°C for Thick and Thin Cells

DRT

A simple DRT analysis was conducted at a regularization parameter of 5 for the cells and the results are shown in Figures 20-23 In the DRT plot, the peaks at a frequency between 0.5-20 Hz vary by the anode thickness as well as the peak between 20-1000 Hz. The 0.5-20 Hz frequency range pertains to gas diffusion at the anode and there is a significant decrease in the resistance which is in agreeance with the Bode plot showing that the concentration overpotential is being avoided/mitigated from the decreased anode thickness (Sumi et al., 2020). The 20-1000Hz frequency range pertains to charge transfer and ionic conduction processes at the anode and although not as significant there is still a decrease in the resistance for the thinner cell implying that the thinning of the anode allows for the electrons to have a less resistive pathway to travel to the external circuit which is in accordance with the results found in the Nyquist plot (Sumi et al., 2020). The catalyst layer thickness is only around ~10-50 μm thick, so although the decreasing of anode thickness will decrease ohmic losses, it is not expected to be as significant as the gas diffusion process (O'Hayre et al., 2016). Additionally, the thin and thick peak for 20-1000 Hz in Figure 20 are almost identical exhibiting that there is no change in ionic conduction between the two thicknesses for that flow rate which is what was observed in Figure 16, furthering the confirmation that that frequency range represents ionic conduction. The other peaks show no sort of consistent trends making it not possible for any conclusion to be drawn from them. There was a significant amount of variation seen in the cathode and buffer layer thickness from the SEM images which supports why there would be inconsistency with the

other peaks. The results of the DRT analysis align most with peak attributions of other mT-SOFCs that are anode supported, but there are results that find the same peaks to attribute to different processes (Hsieh et al., 2015; R. J. Milcarek, Garrett, & Ahn, 2016; Mohammed et al., 2019). This confirms that the peaks and their physical meanings are very dependent on the microstructure of the cell.

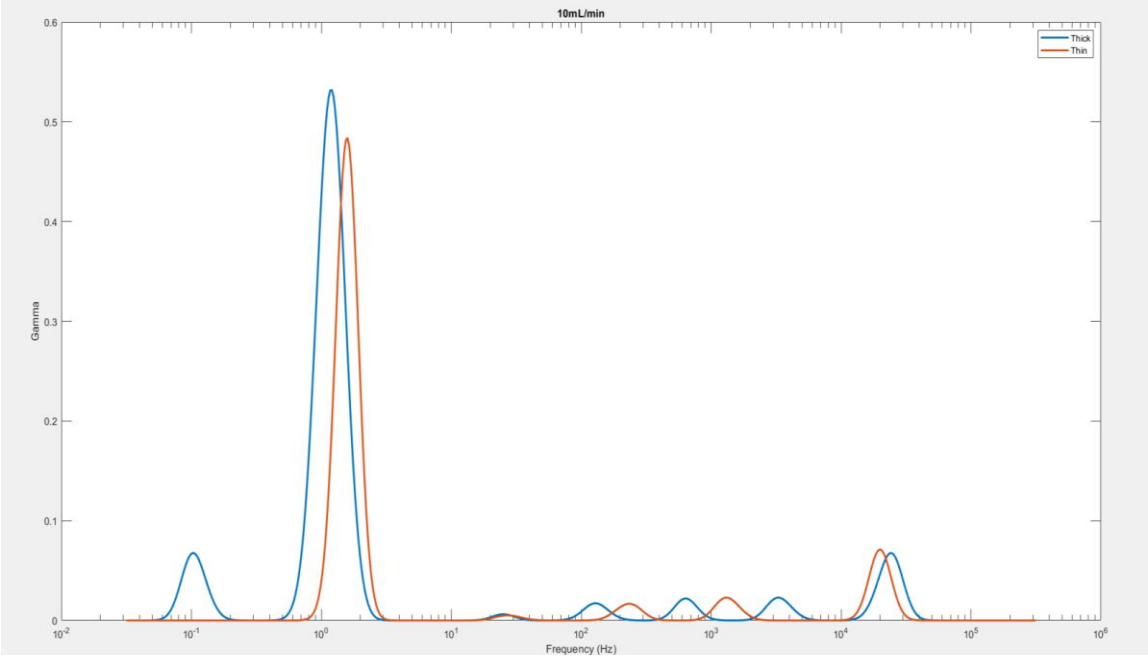

Figure 20: DRT Plot at 10mL/min H_2 at 750°C Regularization Parameter of 5

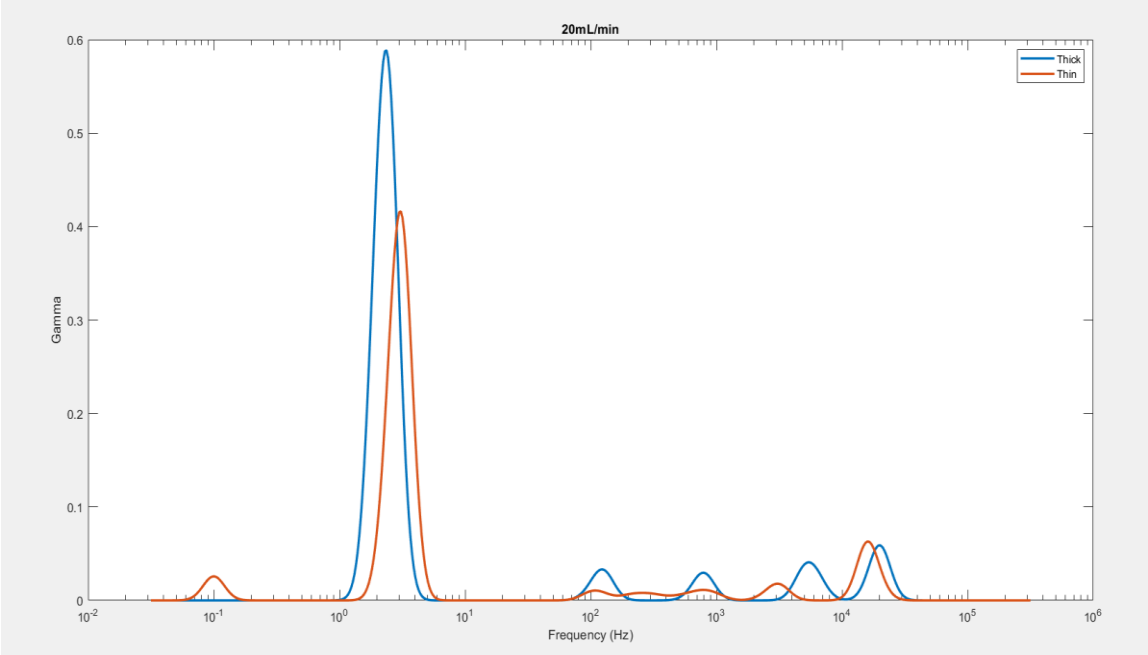

Figure 21: DRT Plot at 20mL/min H_2 at 750°C Regularization Parameter of 5

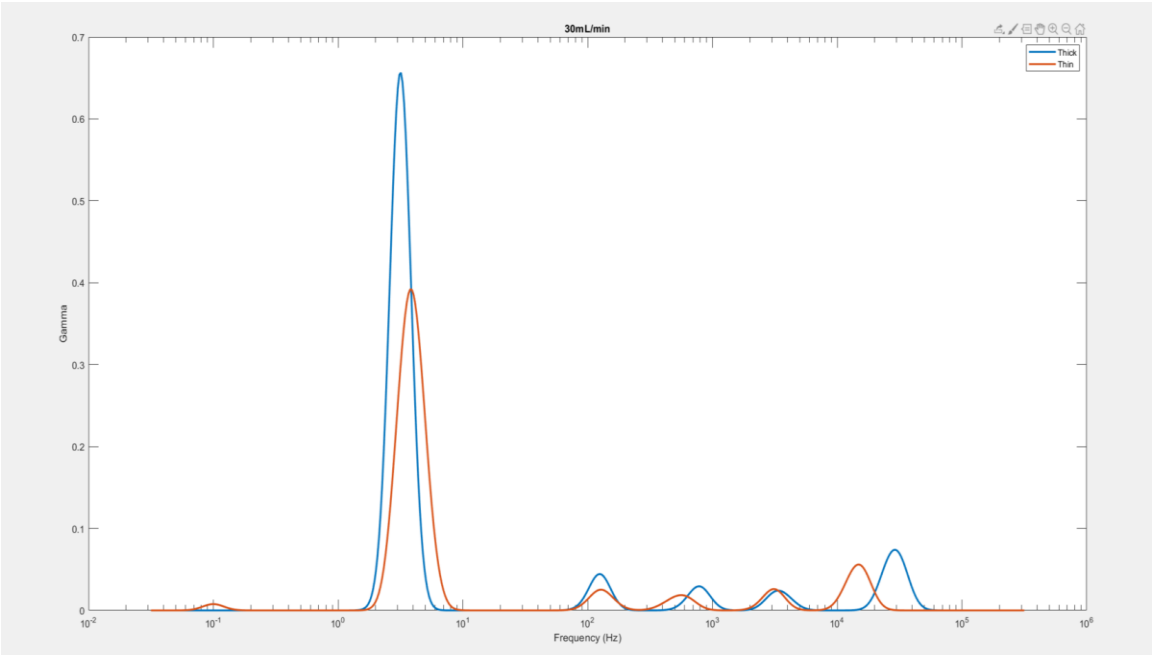

Figure 22: DRT Plot at 30mL/min H_2 at 750°C Regularization Parameter of 5

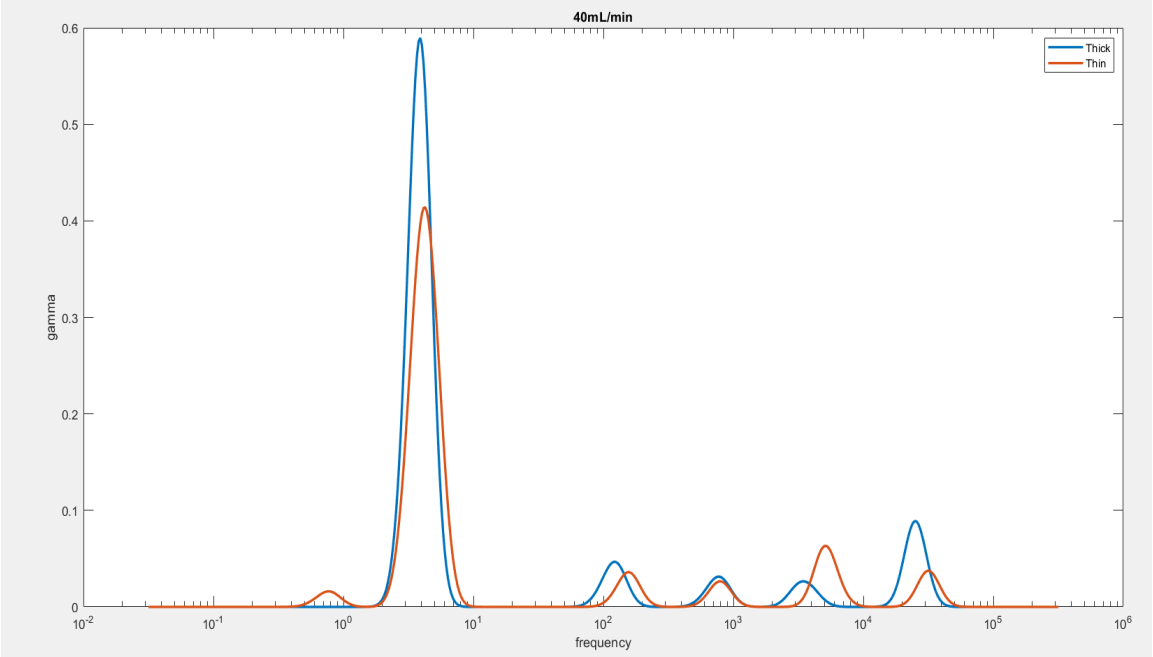

Figure 23: DRT Plot for 40mL/min H_2 at 750°C Regularization Parameter of 5

The tests were repeated on 6 cells, two of each thickness to observe if the results are repeatable and the results are known in Figure 24. The results show that the peaks at 0.5-20 Hz and 20-1000 Hz are consistently getting lower gamma values for the thinner cells in comparison to the thicker cells. This reliability shows the changes in anode thickness directly have impacts on the gas diffusion and charge transfer and ionic conduction processes at the anode (Sumi et al., 2020).

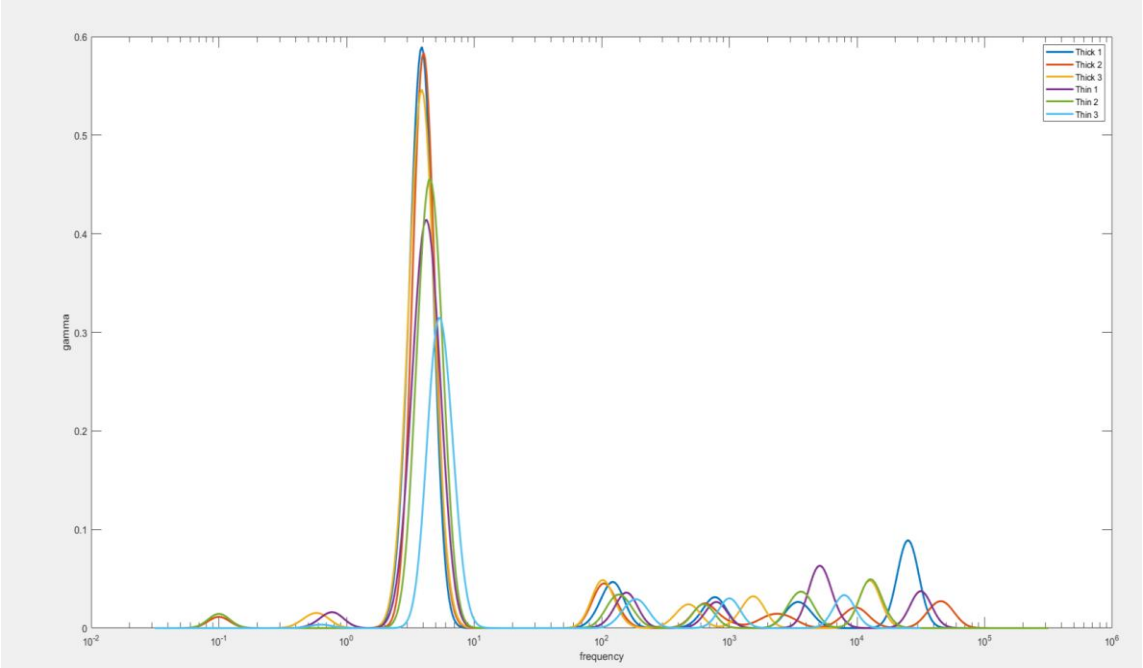

Figure 24: DRT Plot of 6 tests for 40mL/min H_2 at 750°C Regularization Parameter of 5

Uncertainty analysis was conducted to ensure the accuracy and precision of the measured data. The flow meters were verified using a bubble meter and consistent results were achieved within ±3% of the flow rates for this experiment. Polarization curves were run 6 times to be able to calculate the precision error. On average the precision error for the voltage was ± 0.01 V (or ±2.7%). The source meters manufacturing specifications report an accuracy of ± 300 µV for a maximum voltage of 2.0 V. For current, the specs report an accuracy of ± 750 µA for a max current of 1 A. The accuracy of these measurements is fairly high so uncertainty was limited during experiments.

CHAPTER 6

CONCLUSION

Tests were conducted on mT-SOFCs to find the optimized design that would allow them to reach the power density concerns of society today. The power density was only ~50mW/cm^2 higher for the thinner anode cell despite the 500 µm reduction to the diameter. After analyzing SEM images, there was nonuniformity in anode thickness on the same cross-sectional area alluding to errors in the manufacturing process. The Bode and Nyquist plots, however, implicate that there is a consistent reduction in ohmic and mass transport losses pertaining to the decrease in thickness of the anode because there is lower impedance values between the graphs for the frequency regions pertaining to these processes. Additionally, from the DRT analysis the results were able to confirm that the peaks in gamma in the frequency ranges of 0.5-20 Hz and 20-1000 Hz pertain to the anode, found previously in other papers. The 0.5-20 Hz is associated with gas diffusion at the anode and there is a significant decrease in the peak from the thicker cell to the thinner cell. For the 20-1000 Hz peak, it is associated with ionic conduction and charge transfer because although the decrease is not as significant, the peak is higher for all the thicker cells results.

REFERENCES

Alfonso, A. J. D., Freitag, B., Klenov, D., & Allen, L. J. (2010). Atomic-resolution chemical mapping using energy-dispersive x-ray spectroscopy. *Physical Review*, 2–5. https://doi.org/10.1103/PhysRevB.81.100101

Bharti, A., & Natarajan, R. (2022). Proton exchange membrane testing and diagnostics. In *PEM Fuel Cells*. INC. https://doi.org/10.1016/b978-0-12-823708-3.00007-9

Breeze, P. (2017). An Introduction to Fuel Cells. *Fuel Cells*, 1–10. https://doi.org/10.1016/b978-0-08-101039-6.00001-7

Caliandro, P., Nakajo, A., Diethelm, S., & Van, J. (2019). Model-assisted identification of solid oxide cell elementary processes by electrochemical impedance spectroscopy measurements. *Journal of Power Sources*, *436*, 226838. https://doi.org/10.1016/j.jpowsour.2019.226838

Chang, H., Chen, H., Yang, G., Zhou, W., Bai, J., & Li, S. (2019). Enhanced coking resistance of a Ni cermet anode by a chromates protective layer. *Journal of Energy Chemistry*, *37*, 117–125. https://doi.org/10.1016/j.jechem.2018.12.007

Chelmehsara, M. E., & Mahmoudimehr, J. (2018). Techno-economic comparison of anode-supported, cathode-supported, and electrolyte-supported SOFCs. *International Journal of Hydrogen Energy*, *43*(32), 15521–15530. https://doi.org/10.1016/j.ijhydene.2018.06.114

Ciucci, F. (2019). Modeling electrochemical impedance spectroscopy. *Current Opinion in Electrochemistry*, *13*, 132–139. https://doi.org/10.1016/j.coelec.2018.12.003

Ciucci, F., & Chen, C. (2015). Analysis of Electrochemical Impedance Spectroscopy Data Using the Distribution of Relaxation Times : A Bayesian and Hierarchical Bayesian Approach. *Electrochimica Acta*, *167*, 439–454. https://doi.org/10.1016/j.electacta.2015.03.123

Essaghouri, A., Zeng, Z., Zhao, B., Hao, C., Qian, Y., Zhuge, W., & Zhang, Y. (2022). Effects of Radial and Circumferential Flows on Power Density Improvements of Tubular Solid Oxide Fuel Cells. *Energies*, *15*(19). https://doi.org/10.3390/en15197048

Hodjati-Pugh, O., Dhir, A., & Steinberger-Wilckens, R. (2021). The development of current collection in micro-tubular solid oxide fuel cells—a review. *Applied Sciences (Switzerland)*, *11*(3), 1–27. https://doi.org/10.3390/app11031077

Hong, J., Bhardwaj, A., Bae, H., Kim, I., & Song, S. (2020). *Electrochemical Impedance Analysis of SOFC with Transmission Line Model Using Distribution of Relaxation*

Times (DRT) Electrochemical Impedance Analysis of SOFC with Transmission Line Model Using Distribution of Relaxation Times (DRT). https://doi.org/10.1149/1945-7111/aba00f

Hsieh, Y. D., Chan, Y. H., & Shy, S. S. (2015). Effects of pressurization and temperature on power generating characteristics and impedances of anode-supported and electrolyte- supported planar solid oxide fuel cells. *Journal of Power Sources*, *299*, 1–10. https://doi.org/10.1016/j.jpowsour.2015.08.080

Ivers-Tiffée, E., Weber, A., & Herbstritt, D. (2001). Materials and technologies for SOFC-components. *Journal of the European Ceramic Society*, *21*(10–11), 1805–1811. https://doi.org/10.1016/S0955-2219(01)00120-0

Jamil, S. M., Ahmad, S. H., Rahman, M. A., Othman, M. H. D., Rahman, M. A., Jaafar, J., & Ismail, A. F. (2019). Structure formation in anode and its effect on the performance of micro-tubular SOFC: A brief review. *Journal of Membrane Science and Research*, *5*(3), 197–204. https://doi.org/10.22079/JMSR.2018.83592.1187

Jamil, S. M., Othman, M. H. D., Rahman, M. A., Jaafar, J., Ismail, A. F., & Li, K. (2015). Recent fabrication techniques for micro-tubular solid oxide fuel cell support: A review. *Journal of the European Ceramic Society*, *35*(1), 1–22. https://doi.org/10.1016/j.jeurceramsoc.2014.08.034

Lawlor, V., Griesser, S., Buchinger, G., Olabi, A. G., Cordiner, S., & Meissner, D. (2009). Review of the micro-tubular solid oxide fuel cell. Part I. Stack design issues and research activities. *Journal of Power Sources*, *193*(2), 387–399. https://doi.org/10.1016/j.jpowsour.2009.02.085

Liu, J., Ciucci, F., Soc, J. E., Liu, J., & Ciucci, F. (2020). *The Deep-Prior Distribution of Relaxation Times*. https://doi.org/10.1149/1945-7111/ab631a

Liu, M., Chen, C., Liu, M., & Yang, L. (2011). Anode-supported micro-tubular SOFCs fabricated by a phase-inversion and dip-coating process. *International Journal of Hydrogen Energy*, *36*(9), 5604–5610. https://doi.org/10.1016/j.ijhydene.2011.02.016

Liu, T., Wang, Y., Ren, C., Fang, S., Mao, Y., & Chen, F. (2015). Novel light-weight, high-performance anode-supported microtubular solid oxide fuel cells with an active anode functional layer. *Journal of Power Sources*, *293*, 852–858. https://doi.org/10.1016/j.jpowsour.2015.06.018

Malik, V., Srivastava, S., Bhatnagar, M. K., & Vishnoi, M. (2021). Comparative study and analysis between Solid Oxide Fuel Cells (SOFC) and Proton Exchange Membrane (PEM) fuel cell - A review. *Materials Today: Proceedings*, *47*, 2270–2275. https://doi.org/10.1016/j.matpr.2021.04.203

Mccarthy, M. P., Best, M. J., & Betts, R. A. (2010). *Climate change in cities due to global warming and urban effects*. *37*, 1–5. https://doi.org/10.1029/2010GL042845

Milcarek, R., Ahn, J., & Zhang, J. J. (2017). *Review and analysis of fuel cell based, micro cogeneration for residential applications: Current state and future opportunities*. *March*. https://doi.org/10.1080/23744731.2017.1296301

Milcarek, R. J., & Ahn, J. (2018). Rich-burn, flame-assisted fuel cell, quick-mix, lean-burn (RFQL) combustor and power generation. *Journal of Power Sources*, *381*(February), 18–25. https://doi.org/10.1016/j.jpowsour.2018.02.006

Milcarek, R. J., & Ahn, J. (2019). Micro-tubular flame-assisted fuel cells running methane, propane and butane: On soot, efficiency and power density. *Energy*, *169*, 776–782. https://doi.org/10.1016/j.energy.2018.12.098

Milcarek, R. J., & Ahn, J. (2021). Micro-Tubular Solid Oxide Fuel Cell Polarization and Impedance Variation With Thin Porous Samarium-Doped Ceria and Gadolinium-Doped Ceria Buffer Layer Thickness. *Journal of Electrochemical Energy Conversion and Storage*, *18*(2), 1–7. https://doi.org/10.1115/1.4047742

Milcarek, R. J., DeBiase, V. P., & Ahn, J. (2020). Investigation of startup, performance and cycling of a residential furnace integrated with micro-tubular flame-assisted fuel cells for micro-combined heat and power. *Energy*, *196*, 117148. https://doi.org/10.1016/j.energy.2020.117148

Milcarek, R. J., Garrett, M. J., & Ahn, J. (2016). Micro-tubular flame-assisted fuel cell stacks. *International Journal of Hydrogen Energy*, *41*(46), 21489–21496. https://doi.org/10.1016/j.ijhydene.2016.09.005

Milcarek, R. J., Garrett, M. J., Wang, K., & Ahn, J. (2016). Micro-tubular flame-assisted fuel cells running methane. *International Journal of Hydrogen Energy*, *41*(45), 20670–20679. https://doi.org/10.1016/j.ijhydene.2016.08.155

Milcarek, R. J., Garrett, M. J., Welles, T. S., & Ahn, J. (2018). Performance investigation of a micro-tubular flame-assisted fuel cell stack with 3,000 rapid thermal cycles. *Journal of Power Sources*, *394*(April), 86–93. https://doi.org/10.1016/j.jpowsour.2018.05.060

Milcarek, R. J., Nakamura, H., Tezuka, T., Maruta, K., & Ahn, J. (2019). Microcombustion for micro-tubular flame-assisted fuel cell power and heat cogeneration. *Journal of Power Sources*, *413*(October 2018), 191–197. https://doi.org/10.1016/j.jpowsour.2018.12.043

Milcarek, R. J., Wang, K., Falkenstein-Smith, R. L., & Ahn, J. (2016). Performance variation with SDC buffer layer thickness. *International Journal of Hydrogen*

Energy, *41*(22), 9500–9506. https://doi.org/10.1016/j.ijhydene.2016.04.113

Mohammed, H., Al-Othman, A., Nancarrow, P., Tawalbeh, M., & El Haj Assad, M. (2019). Direct hydrocarbon fuel cells: A promising technology for improving energy efficiency. *Energy*, *172*, 207–219. https://doi.org/10.1016/j.energy.2019.01.105

Mutalib, M. A., Rahman, M. A., Othman, M. H. D., Ismail, A. F., & Jaafar, J. (2017). Scanning Electron Microscopy (SEM) and Energy-Dispersive X-ray (EDX) Spectroscopy. In *Membrane Characterization* (pp. 161–179). Elsevier B.V. https://doi.org/10.1016/B978-0-444-63776-5.00009-7

Nguyen, X., Chang, C., Jung, G., Chan, S., Huang, W. C.-W., Hsiao, K.-J., Lee, W.-T., Chang, S.-W., & Kao, I.-C. (2016). Effect of Sintering Temperature and Applied Load on Anode-Supported Electrodes for SOFC Application. *Energies*, *c*. https://doi.org/10.3390/en9090701

O'Hayre, R., Cha, S.-W., Colella, W. G., & Prinz, F. B. (2016). Fuel cell fundamentals. In *Fuel Cell Fundamentals* (Third, pp. 1–580). John Wiley & Sons, Inc. https://doi.org/10.1007/978-0-387-73532-0_1

Ormerod, R. M. (2003). Solid oxide fuel cells. *Chemical Society Reviews*, *32*(1), 17–28. https://doi.org/10.1039/b105764m

Parry V, K. D. (2000). Microscopy : An introduction. *III-Vs Review*, *13*(4), 40–44.

Riley, D. M., Tian, J., Güngör-demirci, G., Phelan, P., Villalobos, J. R., & Milcarek, R. J. (2020). Techno-Economic Assessment of CHP Systems in Wastewater Treatment Plants. *Environments*.

Sammes, N. M., Du, Y., & Bove, R. (2005). Design and fabrication of a 100 W anode supported micro-tubular SOFC stack. *Journal of Power Sources*, *145*(2), 428–434. https://doi.org/10.1016/j.jpowsour.2005.01.079

Skabelund, B. B., Nakamura, H., Tezuka, T., Maruta, K., Ahn, J., & Milcarek, R. J. (2020). Impact of low concentration hydrocarbons in natural gas on thermal partial oxidation in a micro-flow reactor for solid oxide fuel cell applications. *Journal of Power Sources*, *477*(September), 229007. https://doi.org/10.1016/j.jpowsour.2020.229007

Skabelund, B. B., Nakamura, H., Tezuka, T., Maruta, K., Ahn, J., & Milcarek, R. J. (2022). Thermal partial oxidation of n-butane in a micro-flow reactor and solid oxide fuel cell stability assessment. *Energy Conversion and Management*, *254*, 115222. https://doi.org/10.1016/j.enconman.2022.115222

Sumi, H., Shimada, H., Yamaguchi, Y., & Yamaguchi, T. (2020). Degradation evaluation

by distribution of relaxation times analysis for microtubular solid oxide fuel cells. *Electrochimica Acta*, *339*, 135913. https://doi.org/10.1016/j.electacta.2020.135913

Tian, J., & Milcarek, R. J. (2022). Investigating the Influence of Ni, ZrO 2 , and Y 2 O 3 from SOFC Anodes on Siloxane Deposition . *ECS Journal of Solid State Science and Technology*, *11*(4), 044005. https://doi.org/10.1149/2162-8777/ac63e2

Tseronis, K., Kookos, I. K., & Theodoropoulos, C. (2008). *Modelling mass transport in solid oxide fuel cell anodes : a case for a multidimensional dusty gas-based model*. *63*, 5626–5638. https://doi.org/10.1016/j.ces.2008.07.037

Uchida, H., Arisaka, S., & Watanabe, M. (1999). High Performance Electrode for Medium - Temperature Solid Oxide Fuel Cells La (Sr) CoO 3 Cathode with Ceria Interlayer on Zirconia Electrolyte. *Electrochemical and Solid-State Letters*, 428–430.

Yamamoto, O. (2000). Solid oxide fuel cells: Fundamental aspects and prospects. *Electrochimica Acta*, *45*(15–16), 2423–2435. https://doi.org/10.1016/S0013-4686(00)00330-3

Zhang, X., Jin, Y., Li, D., & Xiong, Y. (2021). A review on recent advances in micro-tubular solid oxide fuel cells. *Journal of Power Sources*, *506*(June), 230135. https://doi.org/10.1016/j.jpowsour.2021.230135

Zhao, B., Zeng, Z., Hao, C., & Essaghouri, A. (2022). *A study of mass transfer characteristics of secondary flows in a tubular solid oxide fuel cell for power density improvement*. *May*, 1–19. https://doi.org/10.1002/er.8455

Zhao, T. S., & Xu, C. (2009). Direct Methanol Fuel Cell: Overview Performance and Operational Conditions. *Encyclopedia of Electrochemical Power Sources*, 381–389. https://doi.org/10.1016/B978-044452745-5.00244-6